FE-2727-7
Distribution Category UC-90d

MASS TRANSPORT CHARACTERISTICS OF ZEOLITE CRACKING CATALYSTS

Quarterly Report for the Period
April 1-June 30, 1979

Henry W. Haynes, Jr.

The University of Mississippi
Department of Chemical Engineering
University, Mississippi 38677

Date Submitted - August 30, 1979

PREPARED FOR THE UNITED STATES
DEPARTMENT OF ENERGY

Under Contract No. EF-77-S-01-2727

MASS TRANSPORT CHARACTERISTICS OF ZEOLITE CRACKING CATALYSIS

(FE-2727-7)

ABSTRACT

Previous reports have pointed out the discrepancy between our n-butane/NaY diffusivity measurements and the linear chromatography theory. A series of experiments has been completed which clearly demonstrates the existence of nonlinearities in this system. A similar discrepancy is evident in the system n-hexane/NaY. In contrast, the results for diffusion of 2,2-dimelthylbutane, cyclohexane and t-decalin in zeolite NaY at 280°C are well described by the theory. Surprisingly, no diffusion effects are observed in these systems. The diffusion is too rapid to be detected. The strong adsorption of the high molecular weight hydrocarbons on zeolite NaY makes it difficult to obtain response peaks of sufficient amplitude to give a reliable detector response. It appears that the gas chromatography method cannot give reliable values of the intracystalline diffusivity in these systems.

The cracking of decalin and other hydrocarbons over various acid forms of zeolite -Y has been studied. Arrhenius plots of the first order rate constant for decalin conversion exhibit well-defined break-points indicative of a transition from the kinetics regime to an intracystalline diffusion regime. The temperature at which this break occurs depends upon the activity of the particular zeolite (USY>LaHY>LaNaY). By setting the Thiele modulus equal to unity at the breakpoint it is possible to estimate the diffusivity. This appears to be the first time that values of intracrystalline diffusivity have been reported for a species in a reaction environment.

A series of hydrocracking studies over a NiWHUSY zeolite has been completed. In the first seven yield periods the feed consisted of a mixture of hydrogenated pyrenes. Tetralin was the feed during the remaining six yield periods. Some problems were experienced with temporary plugging during the hydrogenated pyrene runs and the carbon material balances were rather poor. Excellent material balances were obtained during the tetralin runs. The catalyst is quite active for conversion of the hydrogenated pyrenes despite the large molecular size. An analysis of the kinetics is underway.

OBJECTIVES AND SCOPE OF WORK

One objective of this program is to assess the significance of intracrystalline pore diffusion limitations when processing coal-derived syncrudes over zeolite cracking catalysts. The experimental work will involve parallel determinations of mass transport characteristics and catalyst activities using model coal-liquid compounds. A second objective will be to test various zeolite catalysts for their ability to crack coal-derived syncrudes to naphtha.

The purpose of task 1 is to identify the range of critical molecular diameters corresponding to the point at which entrance to sodium zeolite Y crystallites becomes severely restricted at near reaction conditions. In task 2 we will establish the extent to which hydrothermal treatment may affect the intracrystalline diffusivities of high molecular weight hydrocarbons in the hydrogen form of zeolite Y, and the effect of chemical dealumination will be established in task 3. The purpose of task 4 is to test selected zeolite catalysts for their activities and selectivities in cracking model coal-liquid compounds and fractions of coal-derived syncrudes to naphtha under conditions which simulate catalytic cracking. Hydrocracking tests on zeolite-containing catalysts will be conducted in task 5.

SUMMARY OF PROGRESS TO DATE

The chart on the next page summarizes the progress to date. The simulated hydrocracking studies are on schedule. The gas chromatography diffusivity studies have been held up because of our inability until now to explain our results obtained with zeolite NaY. As discussed in the present report, the unavoidable problems with system nonlinearities and strong adsorption phenomena make it difficult or impossible to obtain meaningful intracrystalline diffusivity results with our systems. Further work is planned with the NaY zeolite to verify this conclusion. If we are correct in this assessment, the studies originally planned with the HY and dealuminated HY would be unlikely to yield useful results.

We have deviated somewhat from our planned simulated catalytic cracking studies. Since we have been able to obtain estimates of intracrystalline diffusivities in these experiments, it seems prudent to pursue this approach further. The temperature dependence of these diffusivities can be obtained from experiments on a series of catalysts of varying activity as demonstrated in the present report. Therefore, we propose to substitute experiments on LaHY, LaNaY, etc. zeolite for the dealuminated NH_4Y experiments planned originally.

PROJECT PLAN AND PROGRESS REPORT AS OF 6/30/79

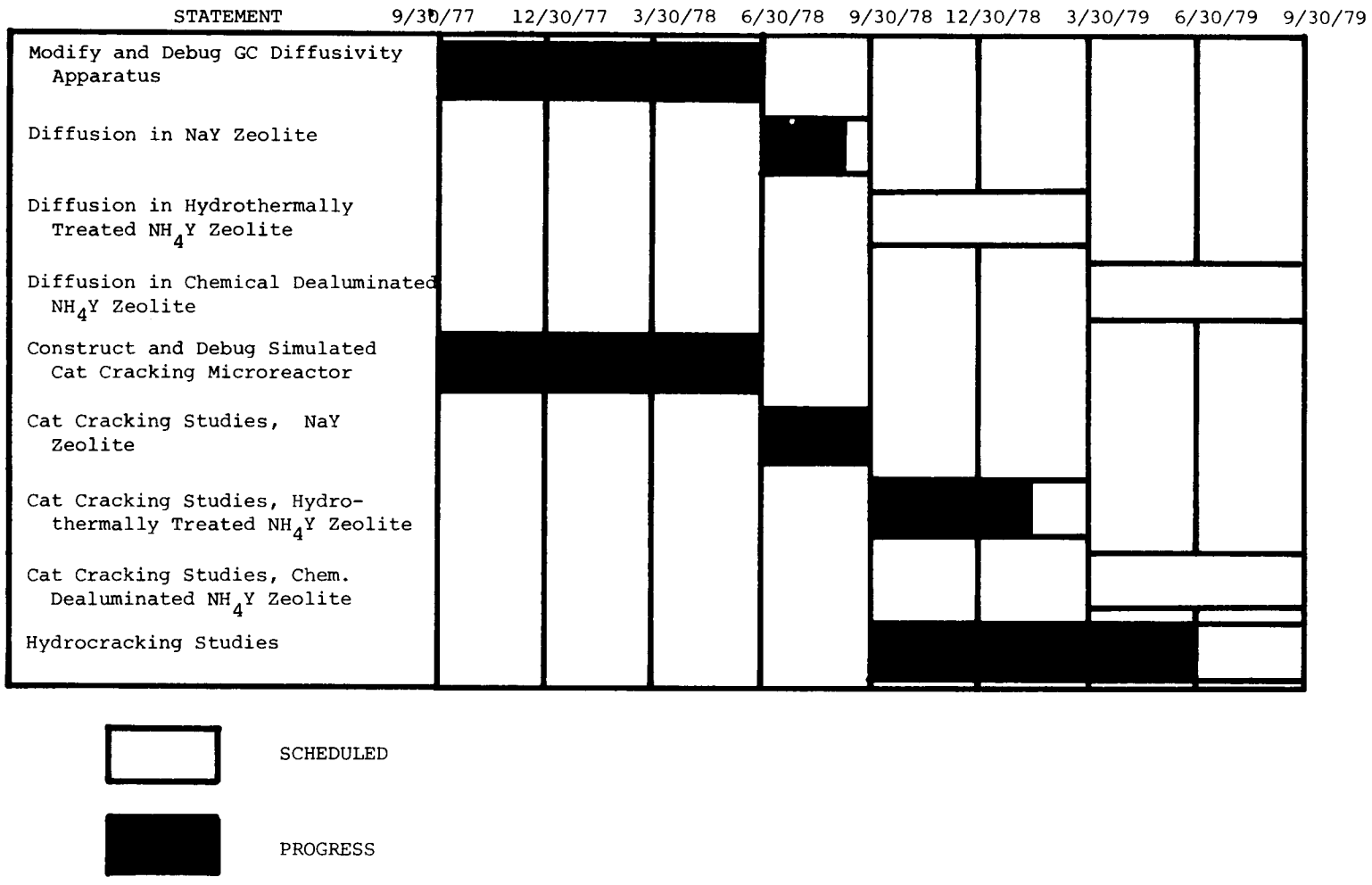

DETAILED DESCRIPTION OF TECHNICAL PROGRESS

In the last quarter additional diffusivity studies on zeolite NaY were completed. New information is provided which bears on the observed discrepancy between theory and experiment that was reported previously. The simulated catalytic cracking studies have progressed. The kinetics model for reaction over zeolite NaY is modified to fit data for strongly adsorbed reactant species. Catalytic cracking over various acidic forms of zeolite Y has also provided some very interesting results. A series of catalytic hydrocracking studies in which a mixture of prehydrogenated pyrenes were hydrocracked over a NiWH-USY zeolite catalyst was completed during the last quarter and preliminary results are contained in this report.

Task 1 - Diffusion Studies in Zeolite NaY - H.W. Haynes, Jr. and Ling-Kai Paul Hsu

In previous reports the inability of the GC-diffusivity model to describe n-butane/NaY diffusion experiments has been pointed out. In the last quarter we took another look at the linearity assumption in this system and the results were quite revealing. The sample injection valve was replaced with a heated injection port and varying amounts of n-butane were injected into the carrier stream by means of a gas-tight syringe. A sharp, arbitrary-shaped pulse was introduced into the column by this technique and both the input and response pulses were recorded on the dual-pen recorder. Since the input pulse did not approximate an impulse, the output pulse was not the desired E-curve or residence time distribution curve. The time domain E-curve was calculated by transforming the experimental input, or X-curve, and output, or Y-curve, into the frequency domain and calculating $E(j\omega) = Y(j\omega)/X(j\omega)$. $E(t)$ was then obtained by computing the inverse Fourier transform of $E(j\omega)$. Filon's method was employed in all the numerical integrations.

The results of a series of these linearity tests are plotted in Fig. 7.1. Column conditions are the same in each of these experiments. Only the n-butane injection volume is varied. Clearly the sample injection volume has a significant influence on the shape of the E-curve for sample volumes larger than about 0.25 ml. The system is nonlinear in this region and the linear chromatography theory would not be expected to apply. The causes of this nonlinearity are unknown at the present time, but likely possibilities include 1. non-Fickian diffusivity, 2. non-linear adsorption isotherm and/or 3. possible heat effects. Single particle heat transfer calculations assuming infinite rates of diffusion appear to rule out the heat effect, although the possibility of a localized heat effect has been suggested (1). We have studied systems characterized by stronger adsorption and larger heats of adsorption which behave linearly

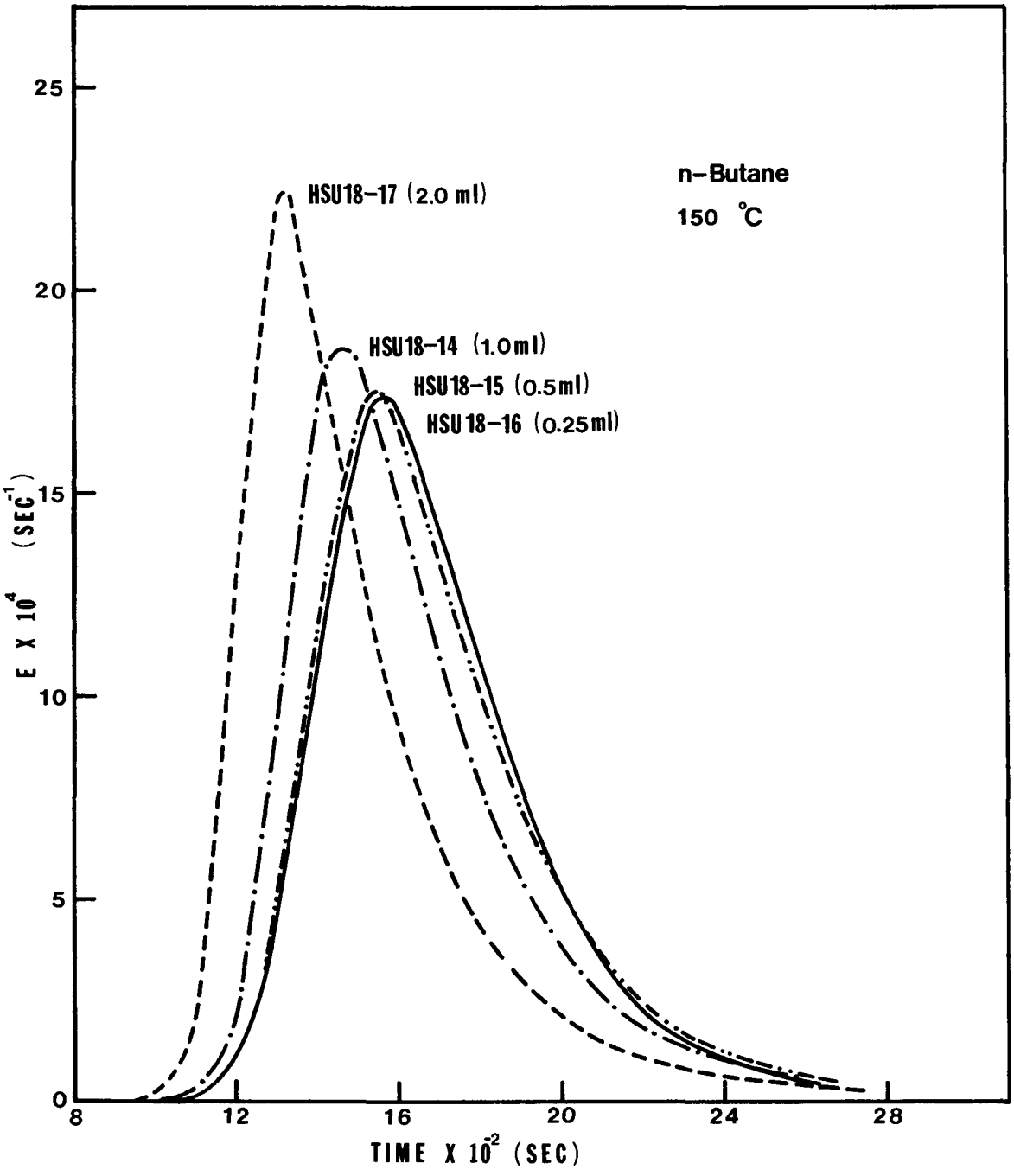

Fig. 7.1. Tests for Linearity in the n-butane/NaY System.

(e.g. cyclohexane/NaY), thus suggesting that the nonlinearity in the n-butane/NaY system is not due to a heat effect. Ruthven reports the diffusion of small molecular species in large pore zeolites (e.g. n-butane in NaX) to be nonlinear even in the Henry's law (linear isotherm) region, but in systems where the molecular and pore opening dimensions are approximately the same the diffusion appear to be linear (2). This observation is at least consistent with our results as the data to follow will indicate.

Referring again to Fig. 7.1, it is apparant that the differences between the E-curves for Runs HSU18-15 and HSU18-16 are not large thus suggesting that the system may be approaching linearity for the smallest injection volume. Unfortunately the output pulse was diluted to such an extent for injection volumes less than 0.25 ml that detector sensitivity became a problem and it was not possible to obtain reliable results in this region. Since Run HSU18-16 represented the closest approach to linearity in this series of experiments, the linear model was fit to these data by the method described in the previous reports. The corresponding E-curve was generated numerically and the results are plotted in Fig. 7.2 for comparison with the experimental curve. The deviations between theory and experiment are very similar in both magnitude and trend to those noted in the earlier experiments which utilized the sample injection valve. From the results plotted in Fig. 7.1 it appears likely that these small, but consistent deviations are due to system nonlinearities. It does not appear possible to obtain precise values of the intracrystalline diffusivity of n-butane in zeolite NaY by the gas chromatography technique because of complications from system nonlinearities. However, we demonstrated earlier that gross deviations between theory and experiment are evident when the intracrystalline diffusion term is removed from the model (3), thus attesting to the importance of this term in the n-butane/NaY system. It would therefore appear that the gas chromatography technique does provide order of magnitude estimates of the intracrystalline diffusivity of n-butane in zeolite NaY under conditions such that the pulse is diluted to the maximum degree as limited by detector sensitivity.

During the last quarter attempts were made to evaluate the diffusivity of large hydrocarbon molecules in zeolite NaY. The apparatus was in the same configuration as just described, i.e. the sample injection port was used instead of the sample valve. Since the second column had been subjected to several thermal cycles, a third column was packed with fresh zeolite NaY. Details of column no. 3 are provided in Table 7.1:

Table 7.1

Column No. 3 Details

Column Length, cm	30.48
Outside Diameter, cm	0.953
Inside Diameter, cm	0.781
Bed Porosity	0.401
Particle Size	40-50 mesh
Avg. Particle Diameter, mm	0.359

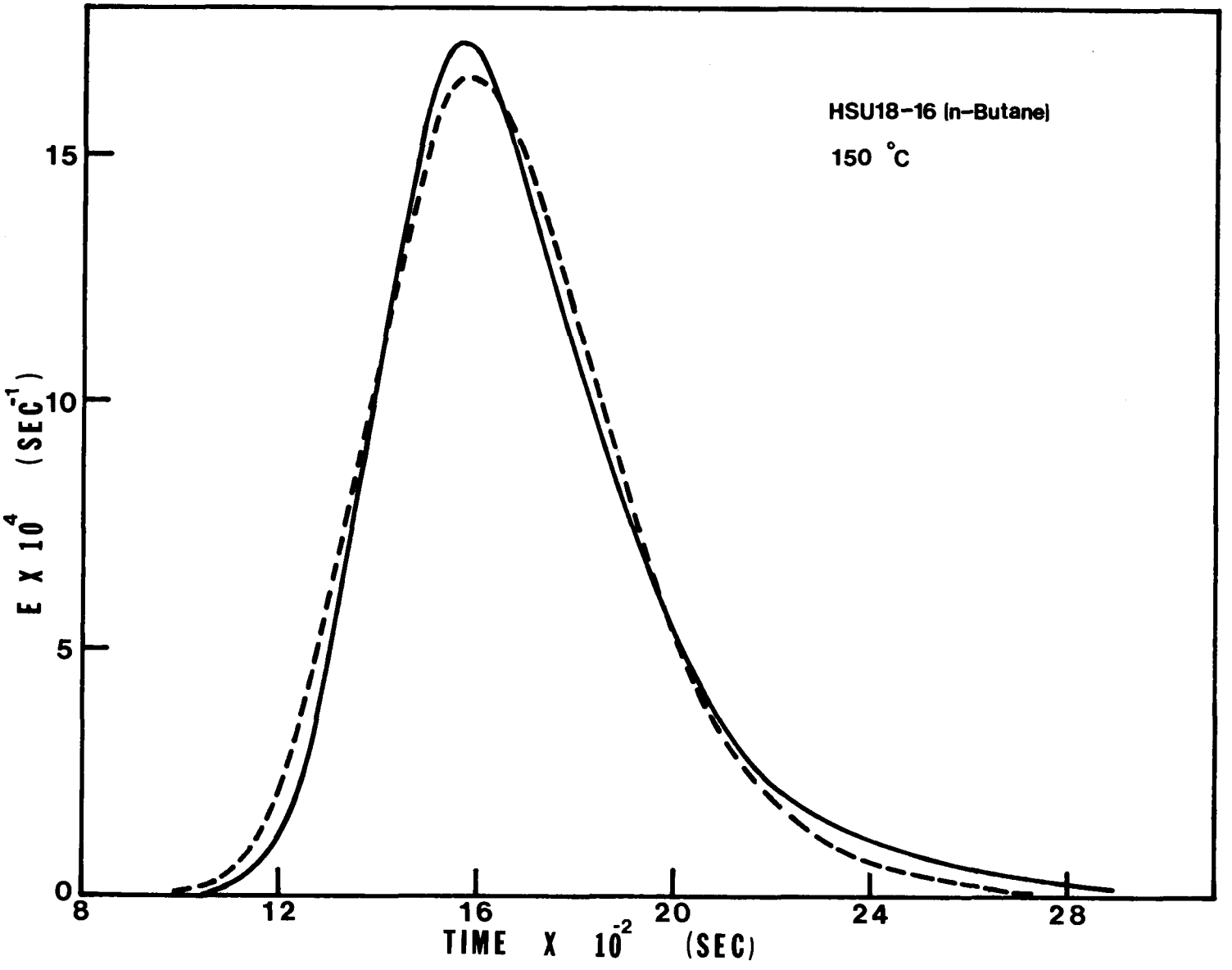

Fig. 7.2. Calculated and Experimental E-Curve for n-Butane Diffusion in Zeolite NaY at 150°C. Solid Curve is Experimental.

It is necessary that a correlation for the axial dispersion coefficient be established before undertaking the diffusion measurements. This was done, as described in the earlier reports, by injecting small molecular species (N_2, CH_4, etc.) into the column and fitting the E-curve to the model with all terms except the adsorption term and the axial dispersion term eliminated. The results are then plotted on a dimensionless plot of Pe vs Re × Sc as illustrated in Fig. 7.3. Surprisingly, when the data for the large hydrocarbon species were treated in this fashion all the points with the possible exception of n-hexane fell on a single curve. Under the conditions of the experiment, i.e. T = 280°C, the diffusion of all these components, again with the possible exception of n-hexane, is too rapid to be detected. As illustrated in Figs. 7.4-7.7 the linear chromatography model provides a much better fit to the experimental results, except for perhaps n-hexane, as compared with the results for n-butane diffusion. This again supports the hypothesis that non-Fickian diffusion is responsible for the nonlinearities experienced with the n-butane/NaY system. The deviations in Fig. 7.4 for n-hexane diffusion are very similar to the deviations observed in the n-butane system. The discrepancy between theory and experiment is not as great, but temperatures are higher, i.e. diffusion is rapid. With the large molecular species it is necessary to operate at high temperatures in order to obtain reasonable elution times. (Note that the elution time for the decalin peak was in excess of 11 hours.) At lower temperatures the output peak is so highly dispersed due to the adsorption term that detector sensitivity becomes a problem.

In summary, it appears that only order of magnitude estimates can be obtained for n-butane diffusion in zeolite NaY at temperatures in the range 125-250°C because of complications from system nonlinearities. Experiments with large molecules at 280°C were entirely consistent with the linear chromatography model, but diffusion was so rapid that no diffusive contributions could be detected. This suggests that non-Fickian diffusion may be responsible for the nonlinearities observed in the n-butane/NaY system. The method is not suitable for measurements of intracrystalline diffusion of very large species such as decalin at temperatures below about 280°C because of the highly dispersed nature of the output pulse and concomitant problems with detector sensitivity.

Task 4 - Simulated Catalytic Cracking Studies - C.Z. Wan

The experimental results from catalytic cracking fused-ring compounds such as decalin over hydrothermally treated faujasite zeolites (ultrastable Y zeolite) and other acidic Y type zeolites (e.g. LaY and LaHY) will be detailed in this report. The results of catalytic cracking of decalin and tetralin over NaY in the absence of carrier gas will also be presented.

I. Catalytic Cracking over NaY Zeolite

In the last report (4), the kinetics analysis was detailed. However,

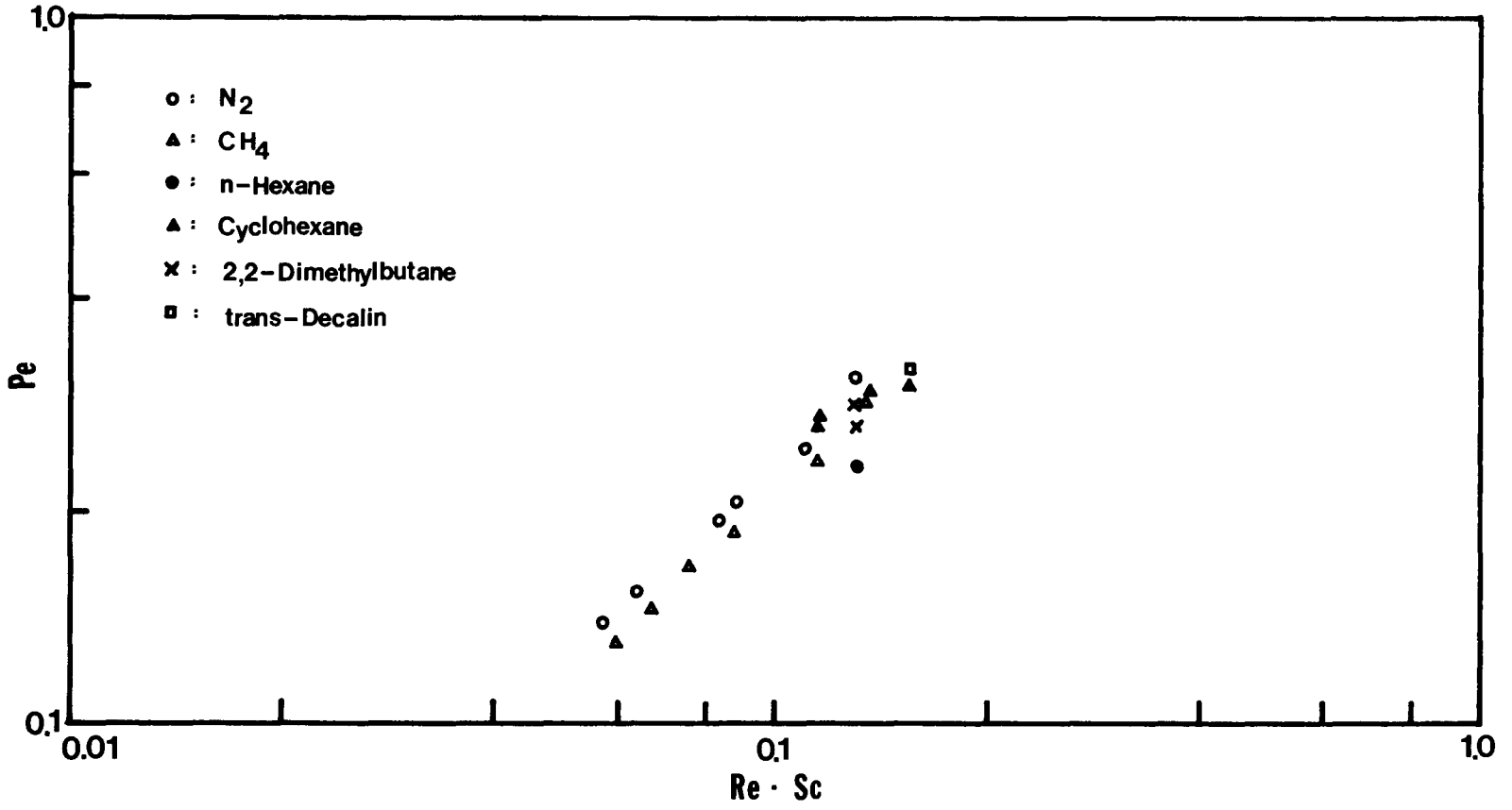

Fig. 7.3 Axial Dispersion Correlation for Column No. 3.

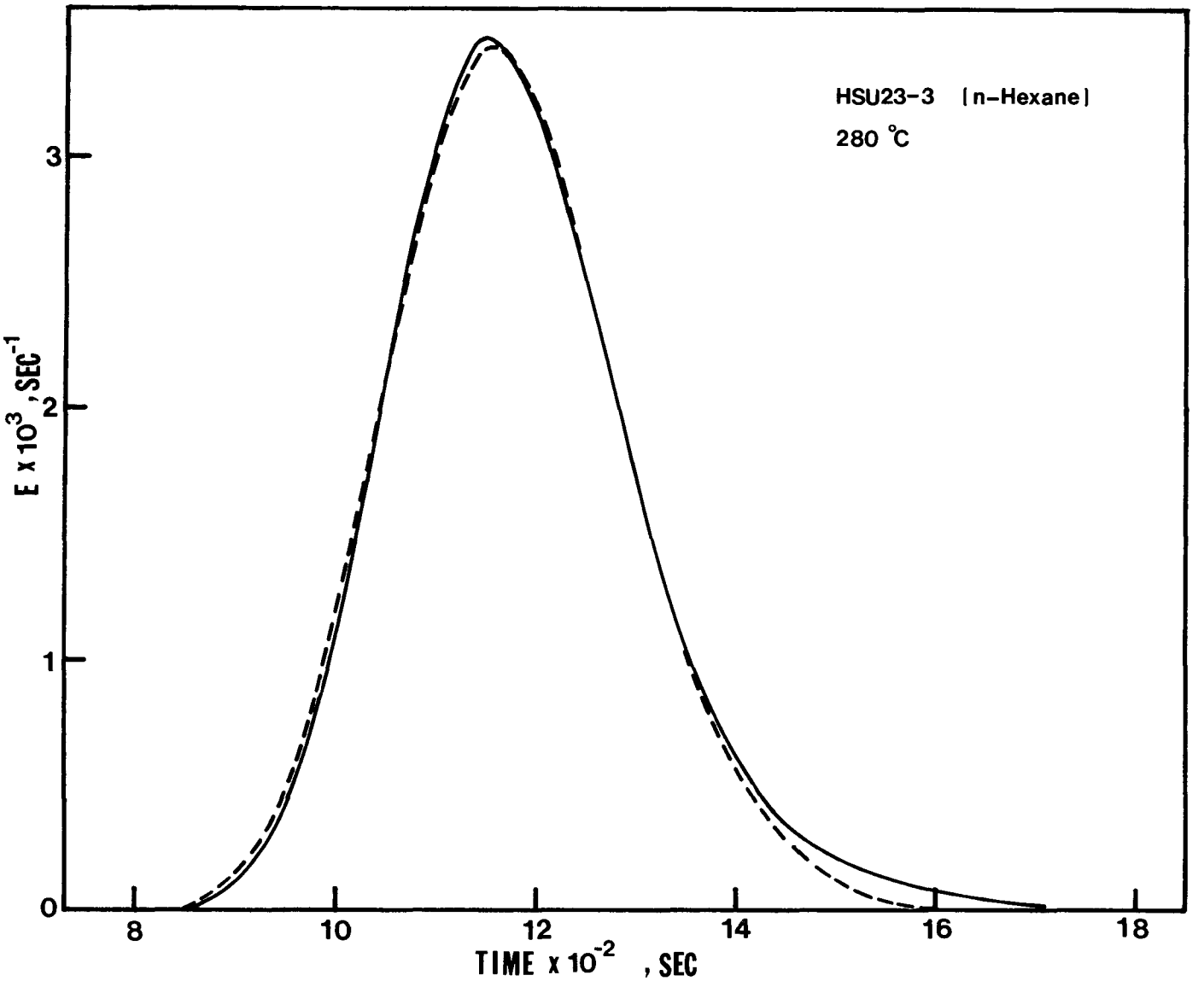

Fig. 7.4. Calculated and Experimental E-Curve for n-Hexane Diffusion in Zeolite NaY at 280°C. Solid Curve is Experimental.

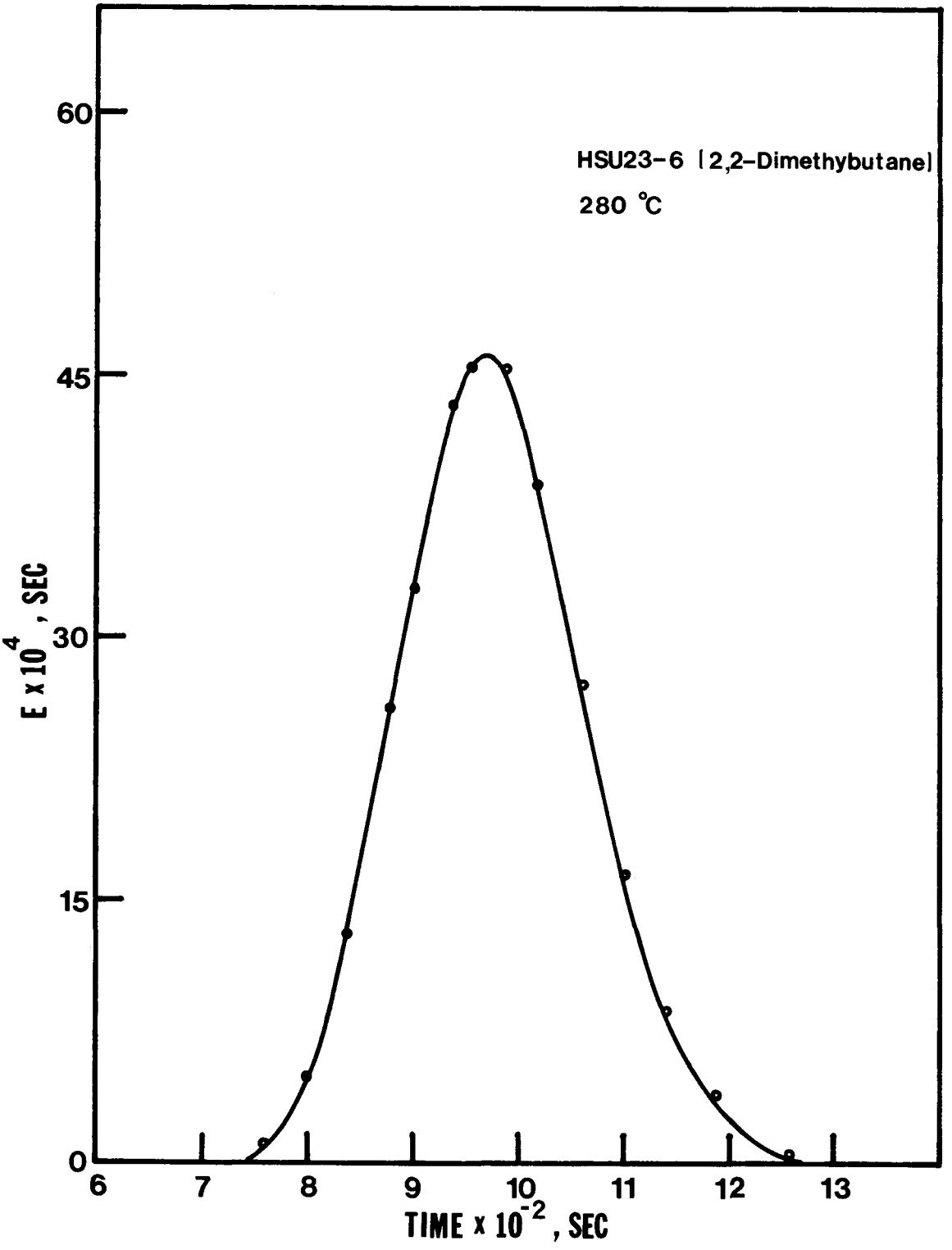

Fig. 7.5. Calculated and Experimental E-Curve for 2,2-Dimethyl-butane Diffusion in Zeolite NaY at 280°C. Solid Curve is Experimental.

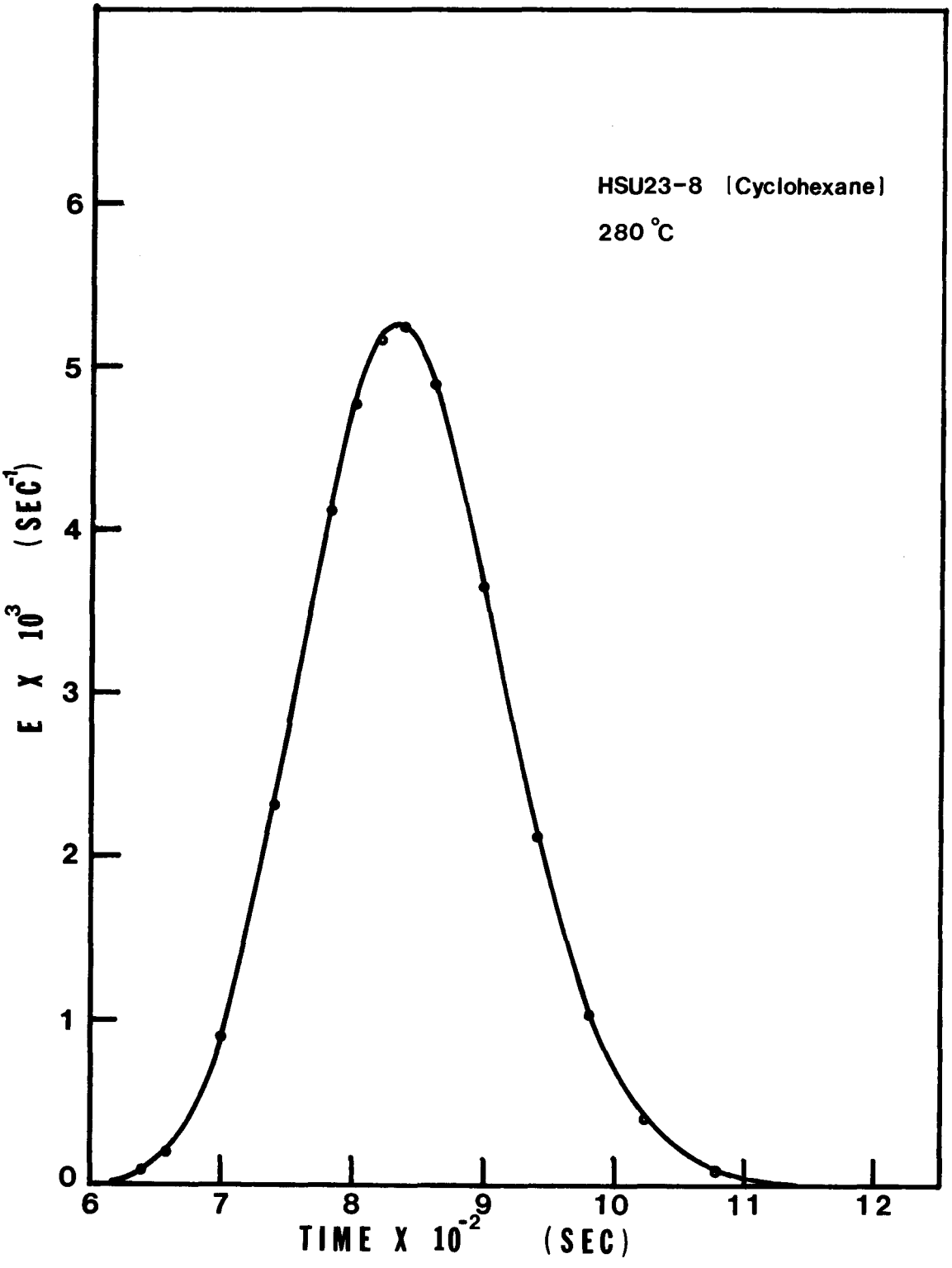

Fig. 7.6. Calculated and Experimental E-Curve for Cyclohexane Diffusion in Zeolite NaY at 280°C. Solid Curve is Experimental.

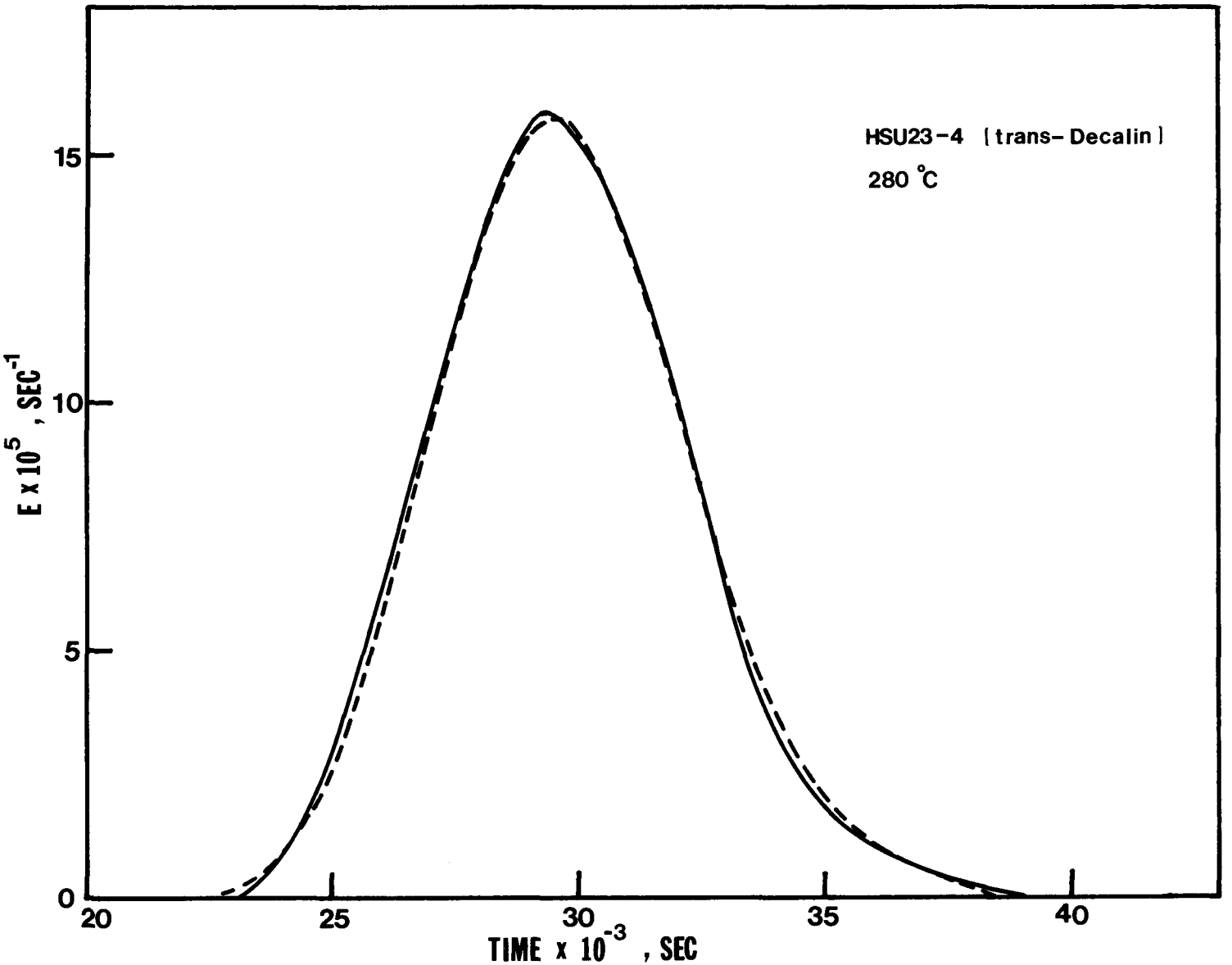

Fig. 7.7. Calculated and Experimental E-Curve for trans-Decalin Diffusion in Zeolite NaY at 280°C. Solid Curve is Experimental.

all the experimental results were calculated and measured when the initial concentration of reactants was about 5% (vol % in vapor) or less. In the last quarter, we ran catalytic cracking experiments where no carrier gas was present in the stream. It was observed that the total conversion of partially hydrogenated compounds such as tetralin differs appreciably when the concentrations of reactants vary as shown in Fig. 7.8. Therefore, the previous analysis of kinetics has to be modified to explain such a phenomenon.

Reaction Kinetics. Through experiments, the total conversion of polycyclic compounds and product compositions for cracking over NaY catalyst indicates the following reaction paths. First, reactant molecules are adsorbed on the catalyst in accordance with the Langmuir adsorption isotherm. On the surface, they are transformed into reactive precursors. Then, the intermediates follow either a cracking conversion which involves α-ring opening, followed by side chain cracking or isomerization, or a dehydrogenation conversion in which the reactant undergoes dehydrogenation within the fused-ring structure without involving any carbon-carbon bond scission. The reaction scheme in this case may be expressed as:

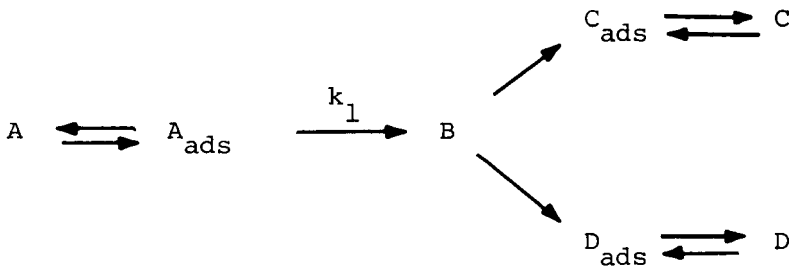

(1)

In the case of slow transformation of surface adsorbed reactant molecules into reactive presursors, the reaction rate can be written as

$$r = \frac{k_1 K_A C_A}{1 + K_A C_A + K_C C_C + K_D C_D} \tag{2}$$

For a plug flow reactor in steady state operation, initial concentration of the reactant can be correlated with the total conversion according to

$$\frac{W}{F} = \int_0^{X_t} \frac{dX_t}{r} \tag{3}$$

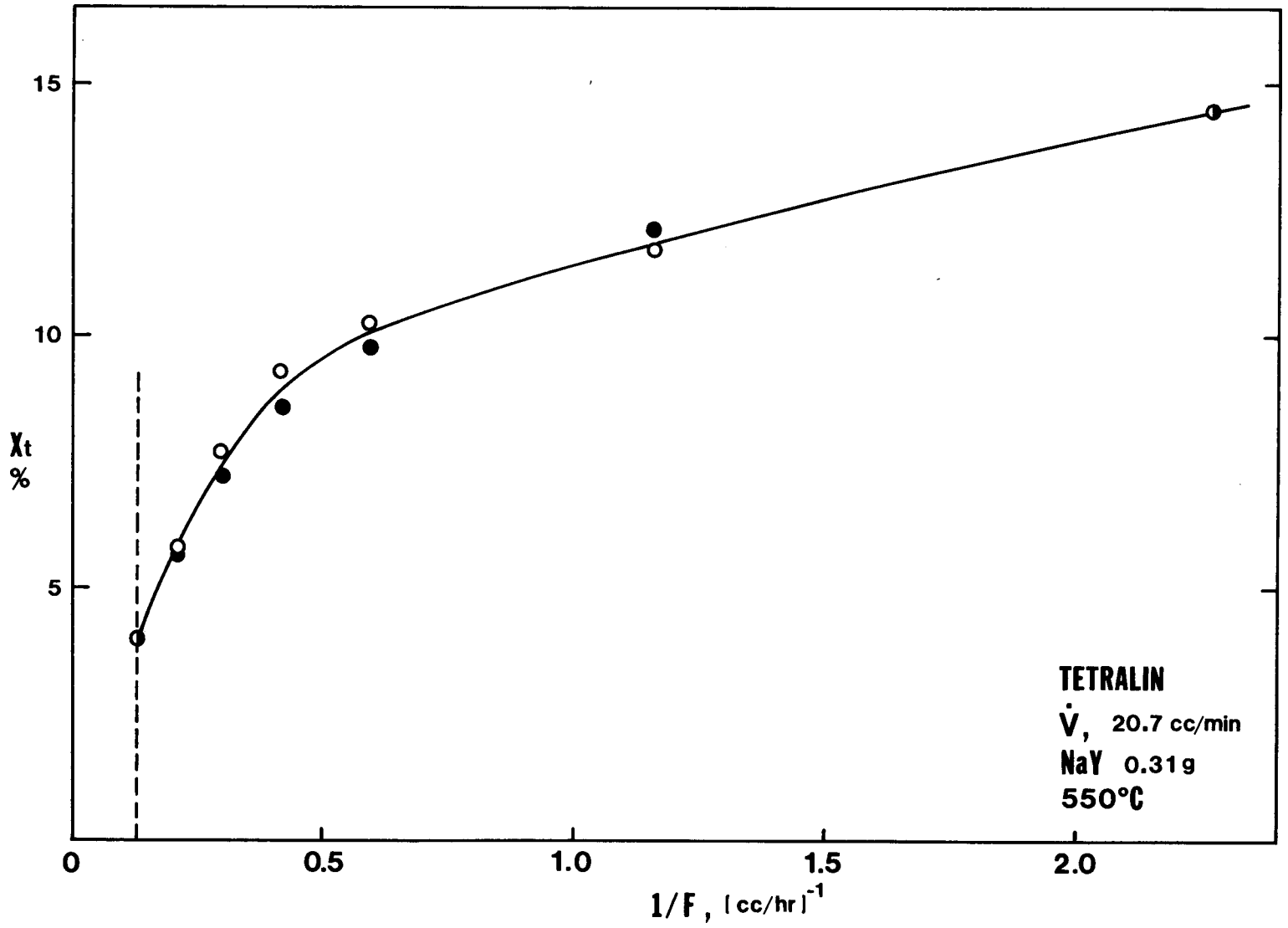

Fig. 7.8. Total Conversion as a Function of Feed Rate. (Total Gas Flow Rate 20.7 cc/min STP).

or

$$\frac{W}{\dot{V}C_A^\circ} = \int_0^{X_t} \frac{(1 + K_A C_A + K_C C_C + K_D C_D)}{k_1 K_A C_A} \, dX_t \tag{4}$$

where W is the weight of catalyst, F is the feed rate, X_t is the total conversion, C_C, C_D are the concentration of cracking and dehydrogenation products respectively, C_A° is the initial concentration of reactant (in terms of vol % in vapor at STP), K_A, K_C, K_D are the dimensionless adsorption equilibrium constants for reactant, cracking product and dehydrogenation product respectively and $\dot{V}$ is the total gas flow rate which is reactant plus helium at STP.

For weak adsorption and little dehydrogenation contribution to the total conversion, K_A, $K_C \ll 1$ and $K_D C_D \ll 1$, then

$$\frac{W}{F} = \frac{1}{C_A^\circ k_1 K_A} \ln \frac{1}{1 - X_t} \tag{5}$$

or

$$k = \frac{\dot{V}}{W} \ln \frac{1}{1 - X_t} \tag{6}$$

The reaction will follow first order kinetics.

For moderately strong adsorption, $K_A > 1$. However, additional variables such as K_C, K_D, C_C, C_D are difficult to determine in this complex system. In our experiments of catalytic cracking of partially hydrogenated fused-ring compounds, it was observed that an amount of moles, which is about equal to the moles of reactant converted, in the total product conserved the fused-ring structure. In addition, if the equilibrium adsorption constants for fused-ring compounds in the products are not differ very much one another, then, Eq. (4) can be approximated as

$$\frac{W}{F} \simeq \int_0^{X_t} \frac{1 + K_A C_A^\circ (1-X_t) + K_A C_A^\circ X_t}{k K_A C_A^\circ (1-X_t)} \, dX_t$$

$$= \int_0^{X_t} \frac{1 + K_A C_A^\circ}{k K_A C_A^\circ (1-X_t)} \, dX_t \tag{7}$$

Thus

$$k = \frac{F}{W} \left(\frac{1 + K_A C_A^\circ}{K_A C_A^\circ}\right) \ln \frac{1}{1 - X_t} \tag{8}$$

or

$$\frac{1}{F \times \ln \frac{1}{1-X_t}} = \frac{1}{kWK_A} \left(\frac{1}{C_A^\circ}\right) + \frac{1}{kW} \tag{9}$$

Equations (8) and (9) will be useful to estimate the adsorption equilibrium constant and overall reaction rate, constants of the partially hydrogenated fused-ring compounds when the total conversion is low and/or the initial concentration of the reactant is low.

In Fig. 7.9, pure decalin (100% vol in vapor) is fed into the system. In this case the contact time is inversely proportional to the liquid feed rate, F. It shows that the total conversion of decalin over NaY can be best described by first order kinetics from which a rate constant of 2.35 g/g-cat/hr at 550°C is calculated. Figure 7.10 shows another example of analysis of kinetics. In this case, decalin is carried into the helium stream and the mixture flows over the reactor bed. The total gas flow rate is kept constant throughout the measurements. Then, the variation of the feed rate, F, is equivalent to a change of initial concentration of decalin in the vapor phase. The concentration has been varied from 5% up to 100% (vol in vapor). The fairly constant value about 2.38 g/g-cat/hr of the overall rate constant indicates that the catalytic cracking of decalin over NaY indeed follows first order kinetics. It also reveals that decalin is not strongly adsorbed on NaY zeolite in the temperatures of interest.

For partially hydrogenated fused-ring compounds such as tetralin, the adsorption on NaY zeolite seems much stronger than that of naphthenes such as decalin. We have replotted the data of Fig. 7.8 following equation (9). For constant total gas flow rate and reaction temperature, the plot of $1/F \ln \frac{1}{1-X_t}$ vs $1/C_A^\circ$ yields a straight line and gives the adsorption equilibrium constant K_A a value of 3.70 at 550°C as shown in Fig. 7.11. In Fig. 7.12 pure tetralin (100 vol % in vapor) is fed into the system.

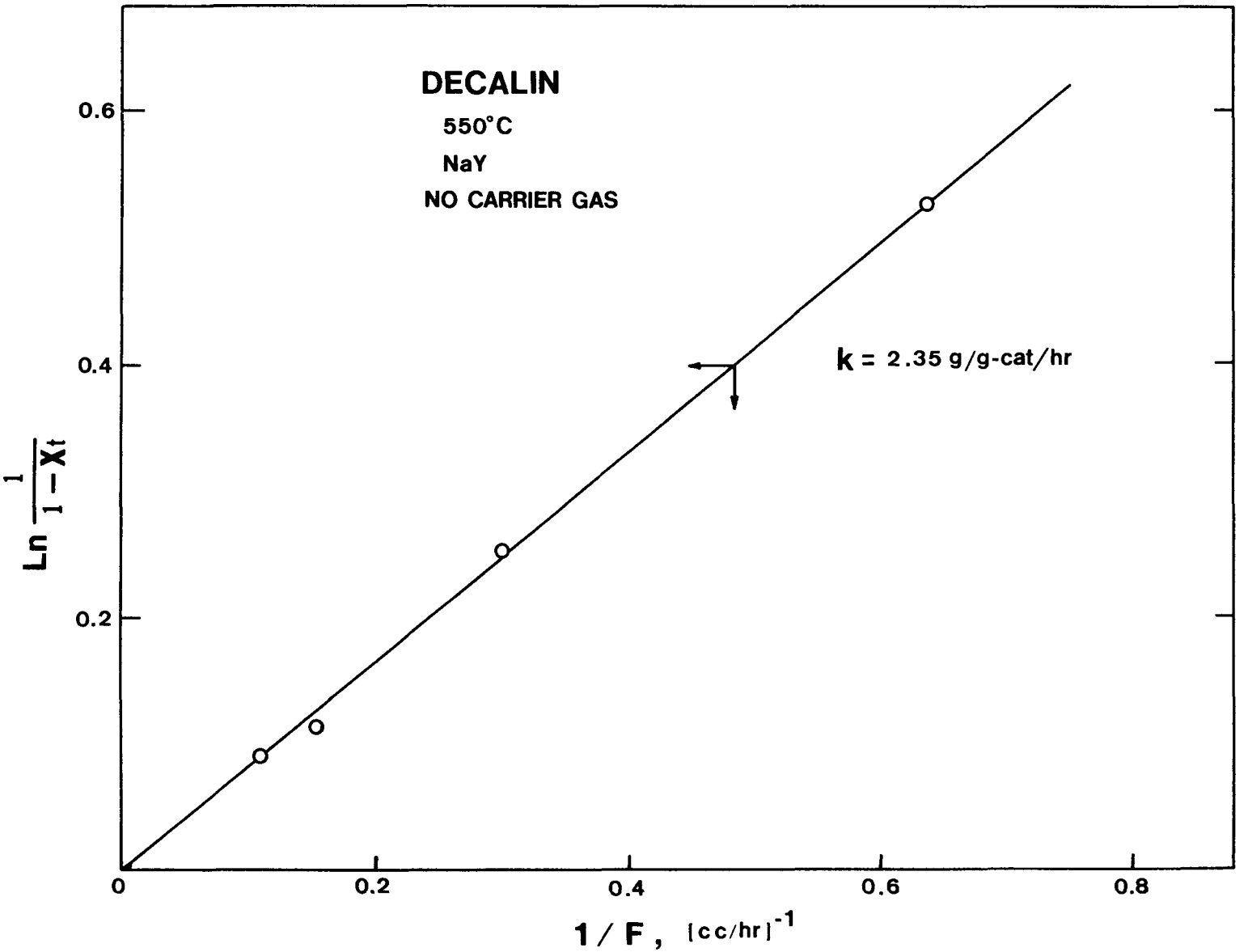

Fig. 7.9. Total Conversion as a Function of Feed Rate for Decalin. Catalyst Weight 0.31g.

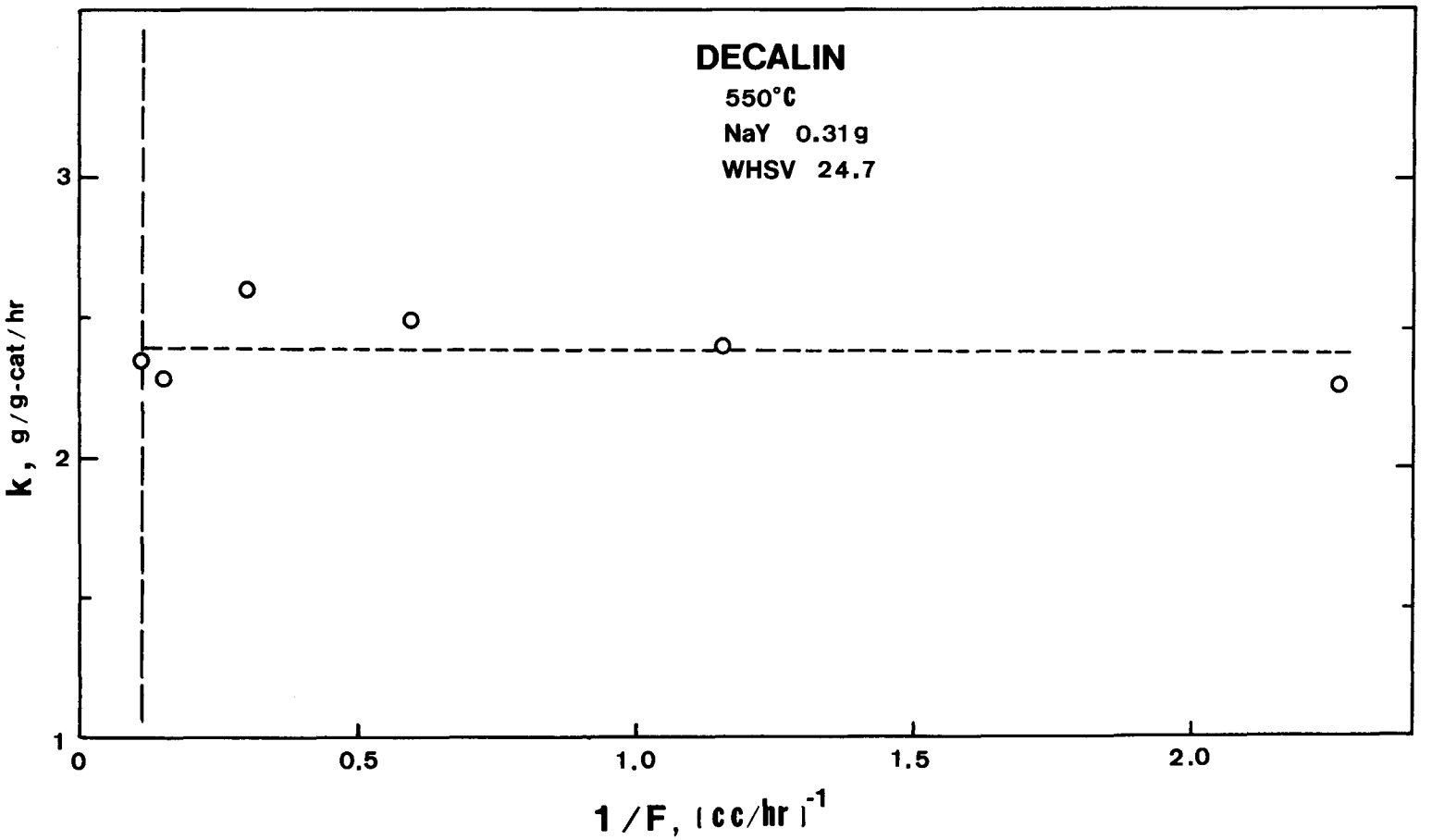

Fig. 7.10. First Order Rate Constant vs Feed Rate.

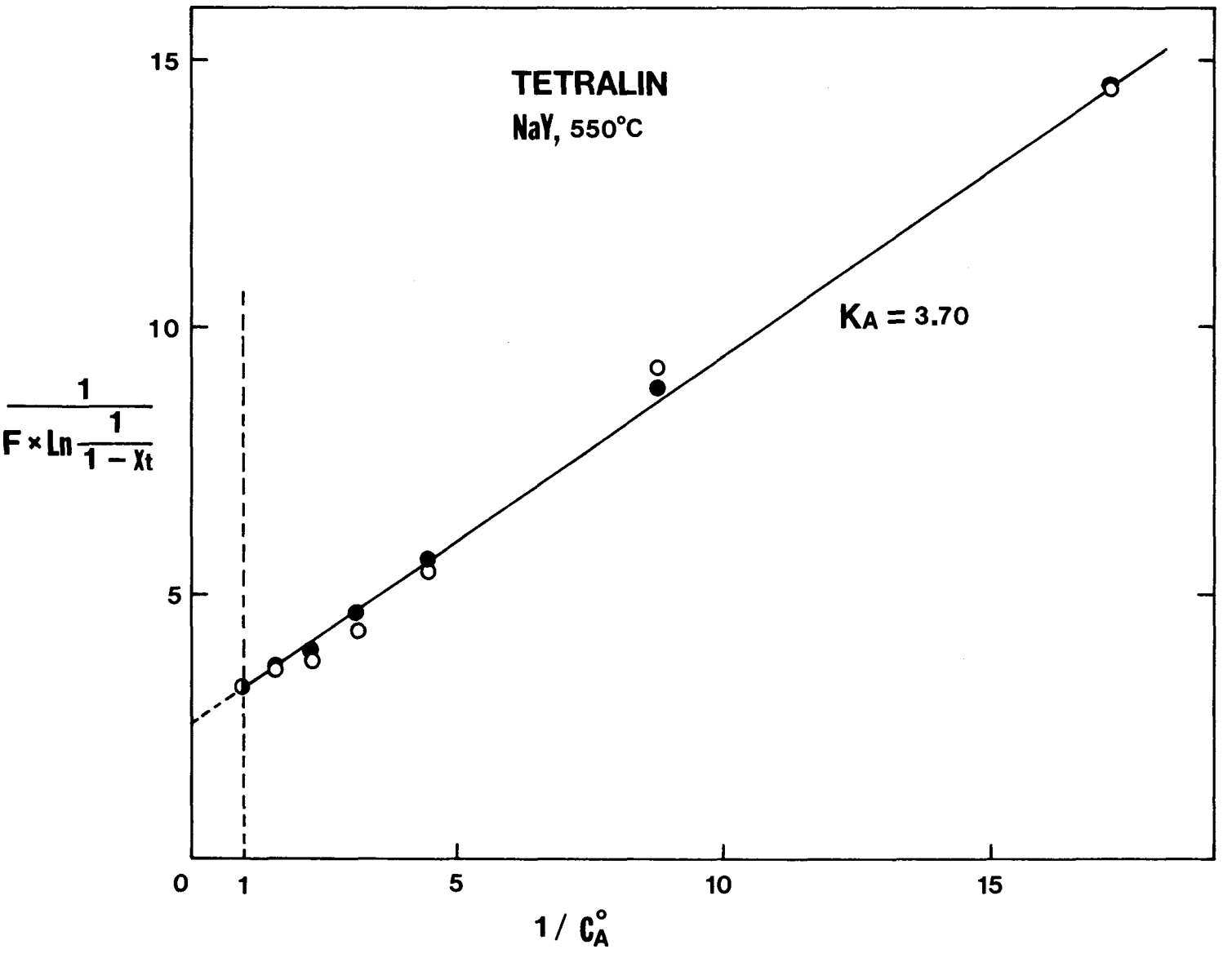

Fig. 7.11. Determination of Adsorption Equilibrium Constant. C_A° in vol% vapor at STP.

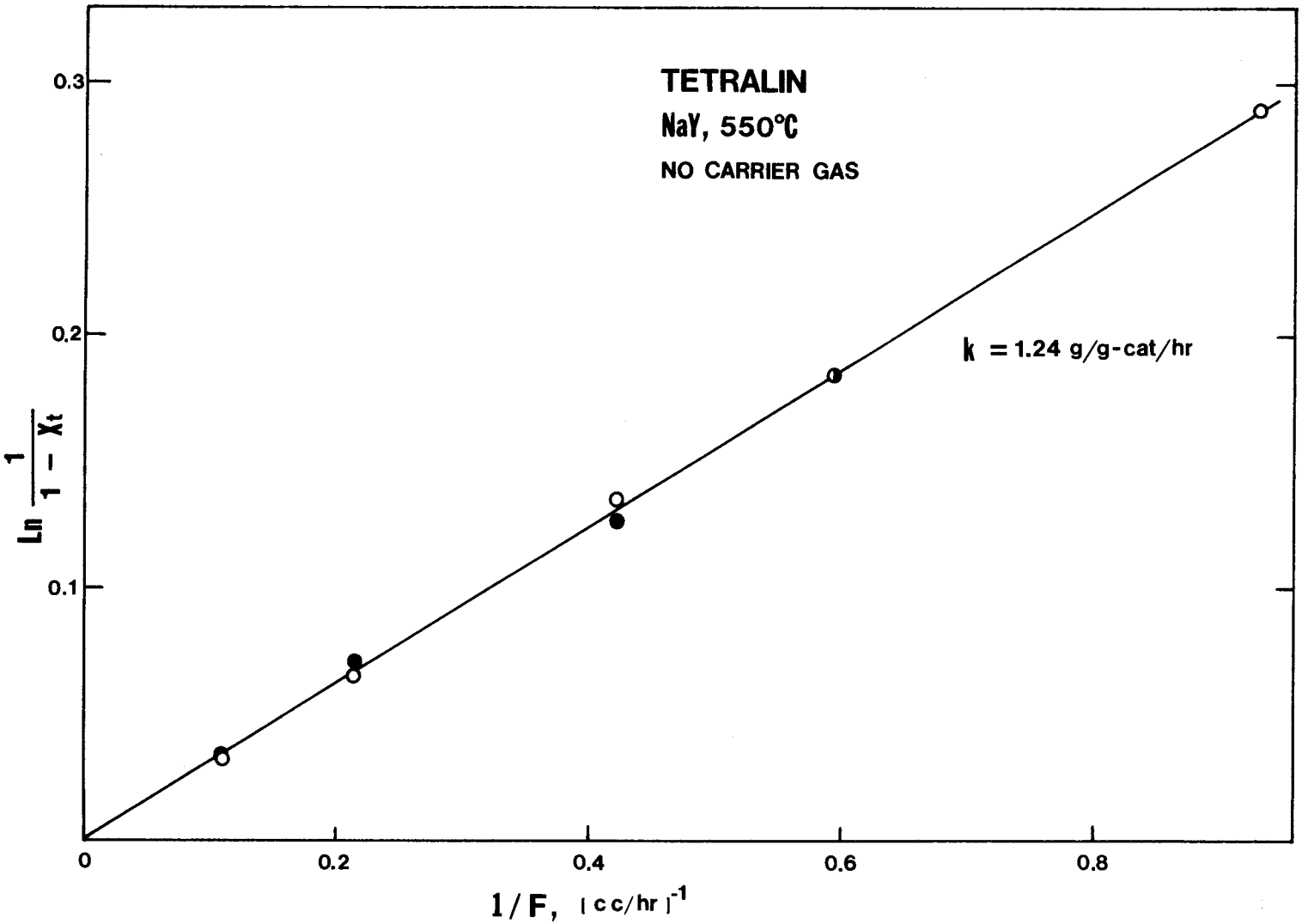

Fig. 7.12. Total Conversion as a Function of Feed Rate for Tetralin.

It shows that the total conversion of tetralin over NaY can be described by the approximate Langmuir reaction kinetics model following Eq. (7) from which a rate constant of 1.24 g/g-cat/hr at 550°C is obtained. The experimental results confirm the reaction scheme described by Eq. (1) over NaY zeolite. Therefore, it is concluded that tetralin is moderately adsorbed over NaY zeolite which complicates the reaction kinetics. Figure 7.13 presents typical Arrhenius plot of overall rate constant of reaction of decalin over NaY. The good linear plot up to 630°C gives the activation energy of catalytic cracking of decalin over NaY of about 55 kcal/mole. This high activation energy indicates that the reaction of decalin is kinetically controlled. Therefore, no significant mass transfer limitation of decalin cracking over NaY are likely.

Product Distribution. Figure 7.14 and Fig. 7.15 present the selectivity plots for decalin and tetralin (both in 100 vol % in vapor) respectively, where X_c and X_d are cracking conversion and dehydrogenation conversion respectively. From the selectivity plots, we can see that in the case of cracking of partially hydrogenated compounds such as tetralin, dehydrogenation contributes more than one third of the total conversion. In Fig. 7.16, the ordinate is mole % of total cracked products. All the measurements for the three compounds shown here are based on a superficial contact time of about one second. This figure is very similar to the results in the previous report (4) except for the product distribution of tetralin. The catalytic cracking of tetralin (100% vol in vapor) over NaY shows that about 88% (mole %) of the total products have the same carbon number as tetralin in which 26% is naphthalene, 56% is methylindan and only 6% undergoes α-ring opening to n-butylbenzene. Therefore, it is concluded that partially hydrogenated fused-ring compounds are very reluctant to crack to small fragments when these compounds are processed over NaY zeolite catalysts.

II. Catalytic Cracking over Acidic Y Type Zeolites

Coke Formation and Product Distribution. As shown in Fig. 7.17 the determination of coke level at different accumulated time-on-stream (indicated above each experimental point) reveals that the quantities of coke formed on the USY catalyst are moderately large which may be due to the acidic nature and extremely high activity of the catalyst. Most of the coke formed, however, is due to the reaction within the initial few minutes time on stream. The activity of the catalyst decreases gradually as the time-on-stream increases. Partially hydrogenated fused-ring compounds such as tetralin seem to have lower activity but higher coking rates when compared with their counterparts - naphthenes. Similar decay patterns at different reaction temperatures have also been observed. Therefore, if the reaction kinetics is to be analyzed in the steady state operation in our experiments, the reaction time-on-stream must be kept to a constant value for all the measurements in order to compare the activities of the catalysts.

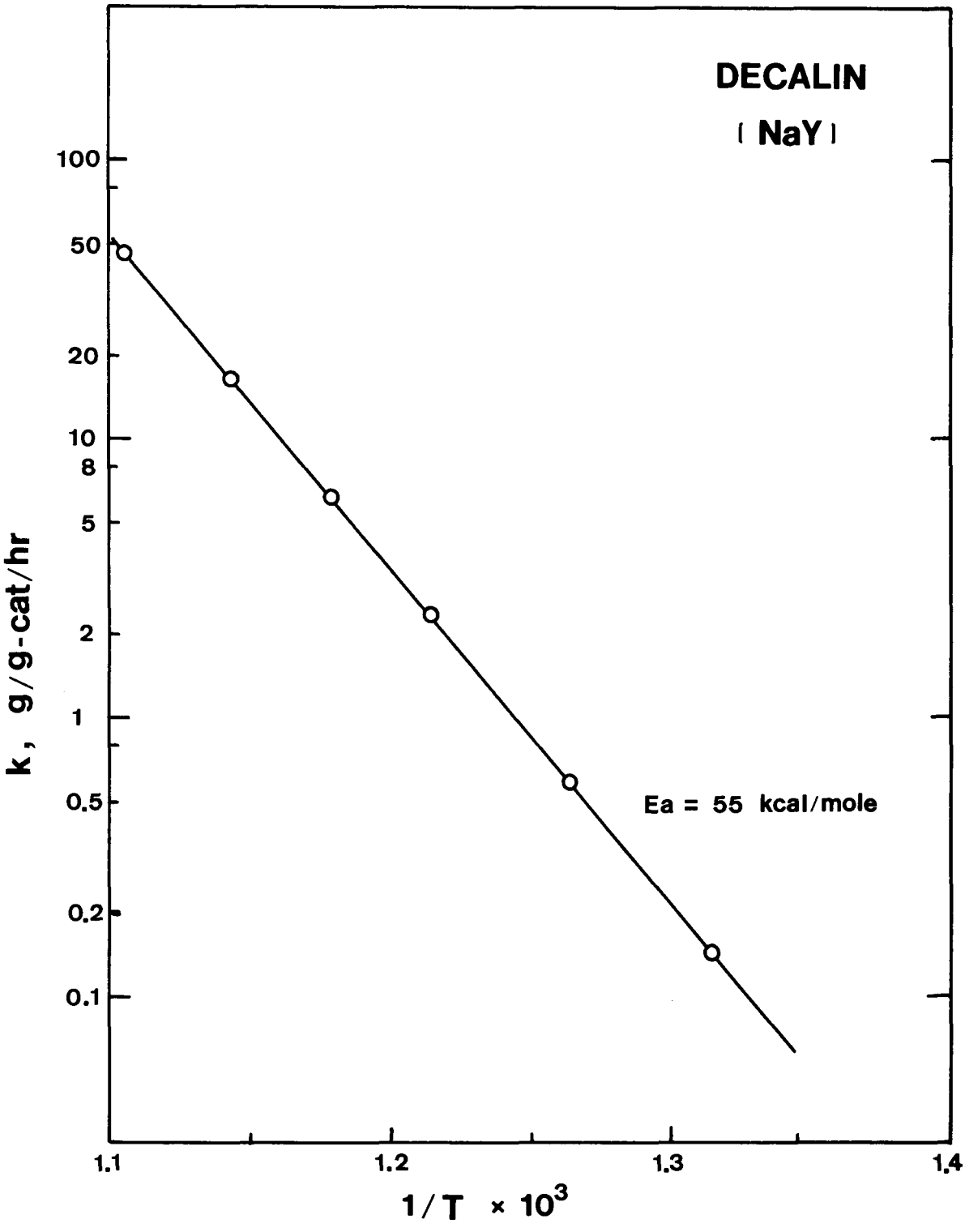

Fig. 7.13. First Order Rate Constant as a Function of Temperature for Decalin.

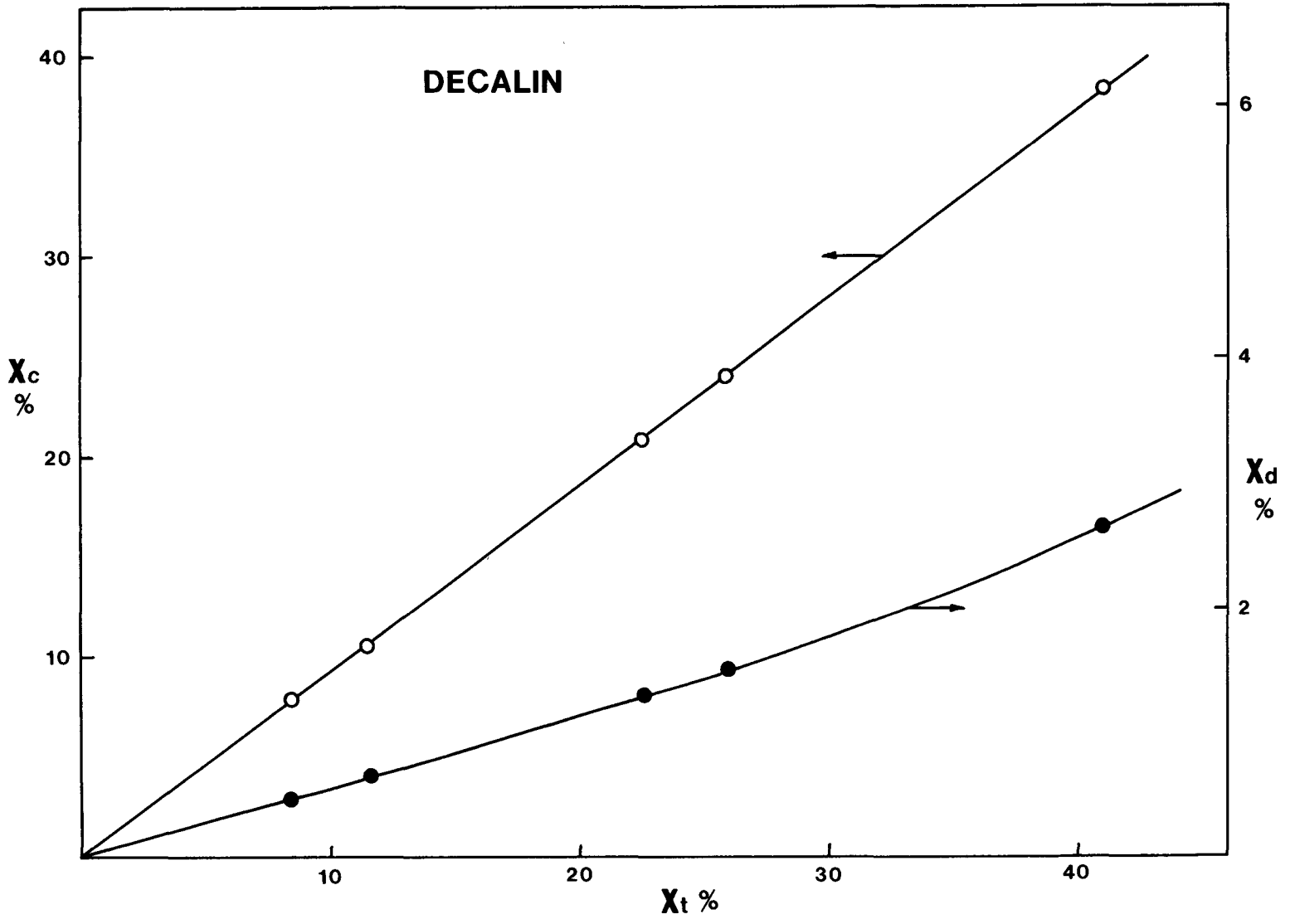

Fig. 7.14. Selectivity Plot for Decalin over NaY at 550°C.

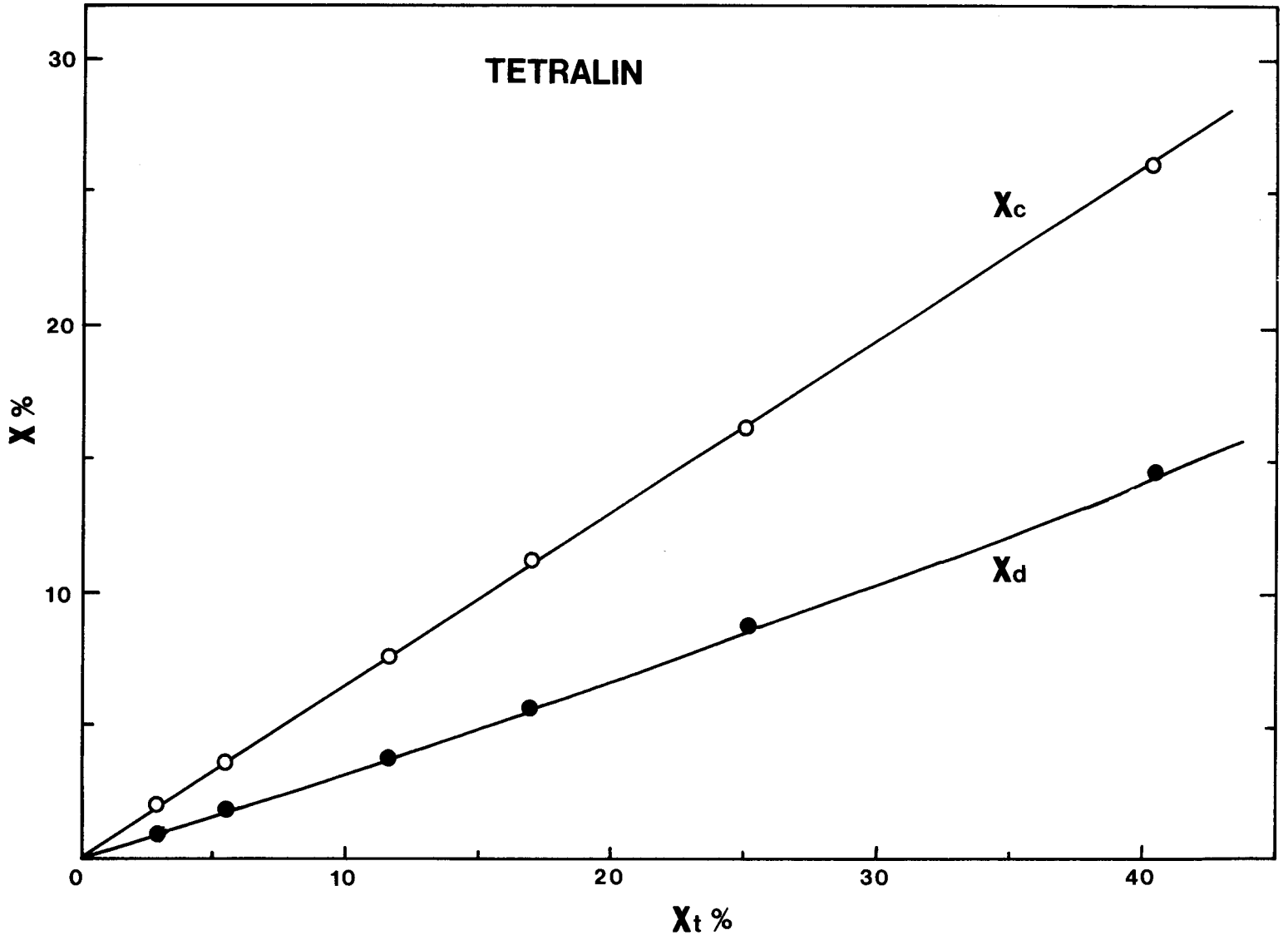

Fig. 7.15. Selectivity Plot for Tetralin over NaY at 550°C.

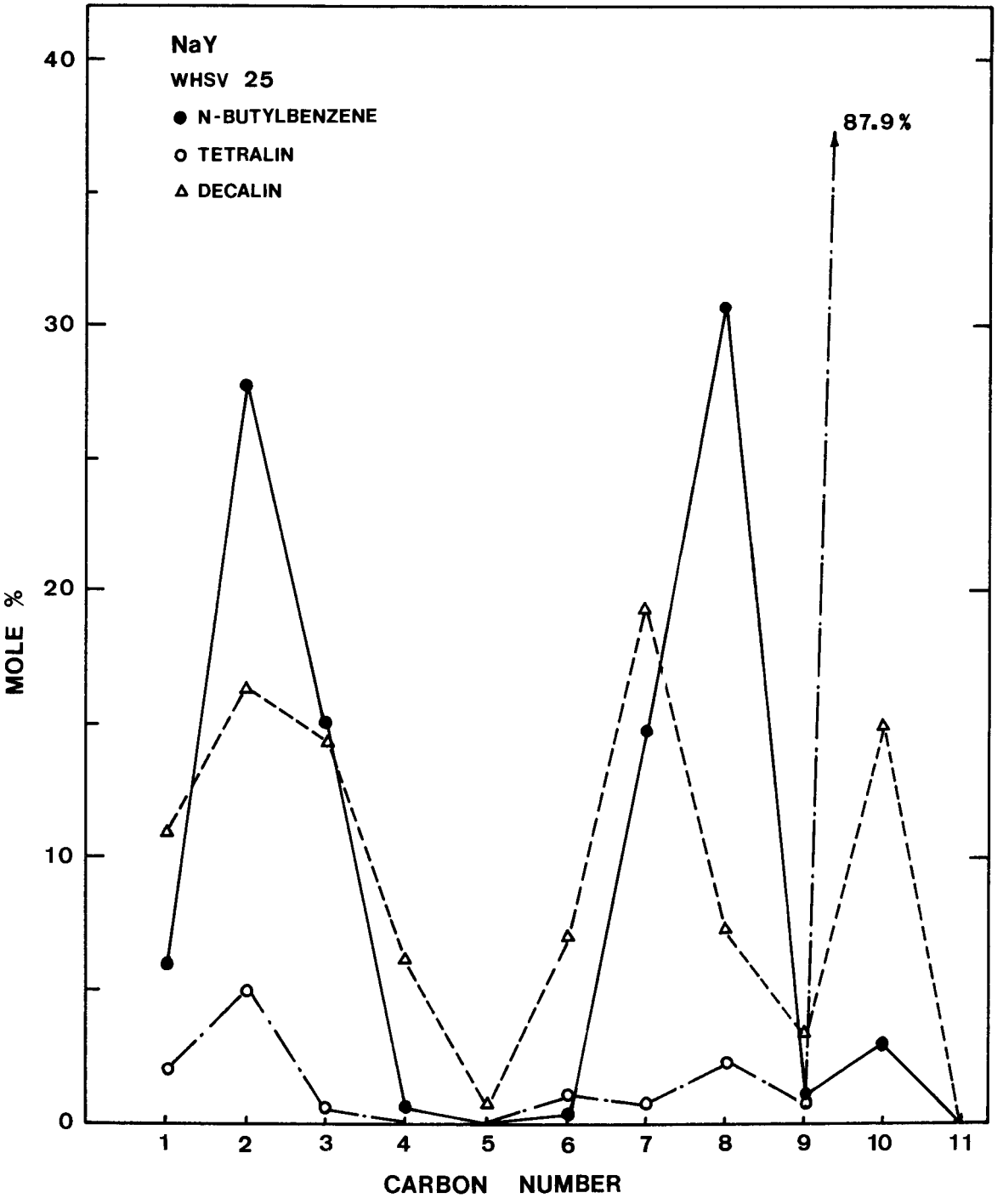

Fig. 7.16. Product Distribution over NaY.

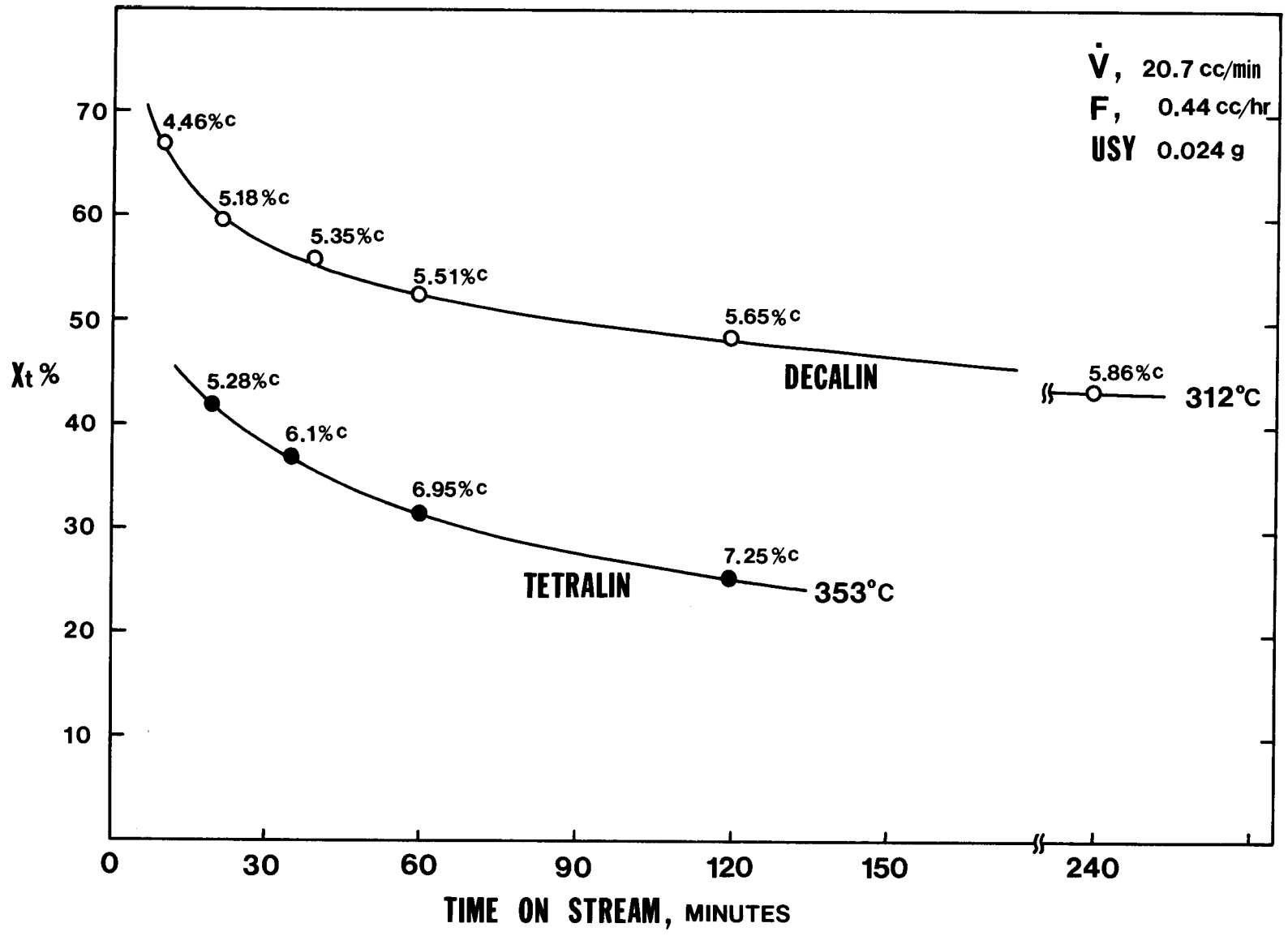

Fig. 7.17. Catalyst Activity as a Function of Time-on-Stream over USY Zeolite.

The catalytic cracking of saturated hydrocarbons and naphthenes over acidic zeolite catalysts has been reported to follow first order kinetics (5). The catalytic cracking of partially hydrogenated fused-ring compounds over non-acidic zeolite has been found to be more complex. The catalytic cracking of partially hydrogenated fused-ring compounds over acidic zeolites may also be complex. In order not to get too much complexity, we are not going to discuss the kinetics of partially hydrogenated fused-ring compounds over acidic zeolite catalysts.

Over acidic zeolites such as USY, the catalytic cracking pattern is completely different from that over NaY. This may be attributed to the completely different reaction mechanisms. In Fig. 7.18, the ordinate is mole % of total cracking product. All the measurements for decalin and tetralin are based on a superficial contact time* of one second and a total time-on-stream of 40 minutes. The additional reaction conditions are collected in Table 7.2. It shows that 55% of the products from cracking of decalin is cyclopentane or cyclohexane derivatives C_9 compounds, 25% is the C_{10} compounds in which 22% is cyclohexane or benzene derivatives and 3% is the product from dehydrogenation of the fused ring. Gases and higher carbon number compounds are found in very small quantity. In the case of cracking of tetralin, it is found that about 62% of the total products has the same carbon number as tetralin in which 36% is naphthalene, 13% is methylindan and the other 13% is benzene derivatives. In addition, 13% benzene and another 15% higher carbon number compounds are found in the total products. Gases are present in negligible amount. Therefore, it seems that the partially hydrogenated fused-ring compounds are also very reluctant to crack to small fragment when these compounds are processed over acidic faujasite catalysts.

Mass Transfer Limitation. In order to observe the mass transfer limitation of cracking of decalin over USY zeolite, a reference reaction over an amorphous acidic catalyst (silica-alumina) is made for comparison. We have shown that more than 95% of the cracking activity observed in NaY zeolite is the result of reaction within the zeolite crystallites by comparing the reaction over NaY and NaA catalysts. Therefore, it is quite reasonable to use this inference to the acidic faujasite zeolites also. Figure 7.19 presents the Arrhenius plot of first order rate constants of decalin and n-butylbenzene over silica-alumina catalyst. Each activity measurement is based on a reaction of 40 minutes time-on-stream. In a kinetically controlled region, the activation energy for the reaction of decalin is about 22 kcal/mole and activation energy for n-butylbenzene is about 30 kcal/mole. Because the reaction mechanisms of decalin over silica-alumina catalyst and USY zeolites are essentially similar (both are acidic catalysts), it is reasonable to infer that activation energy for decalin cracking over USY zeolites in a kinetically controlled region

---

*Superficial contact time is defined as volume of the catalyst (c.c.) divided by the total gas flow rate (c.c./sec., STP).

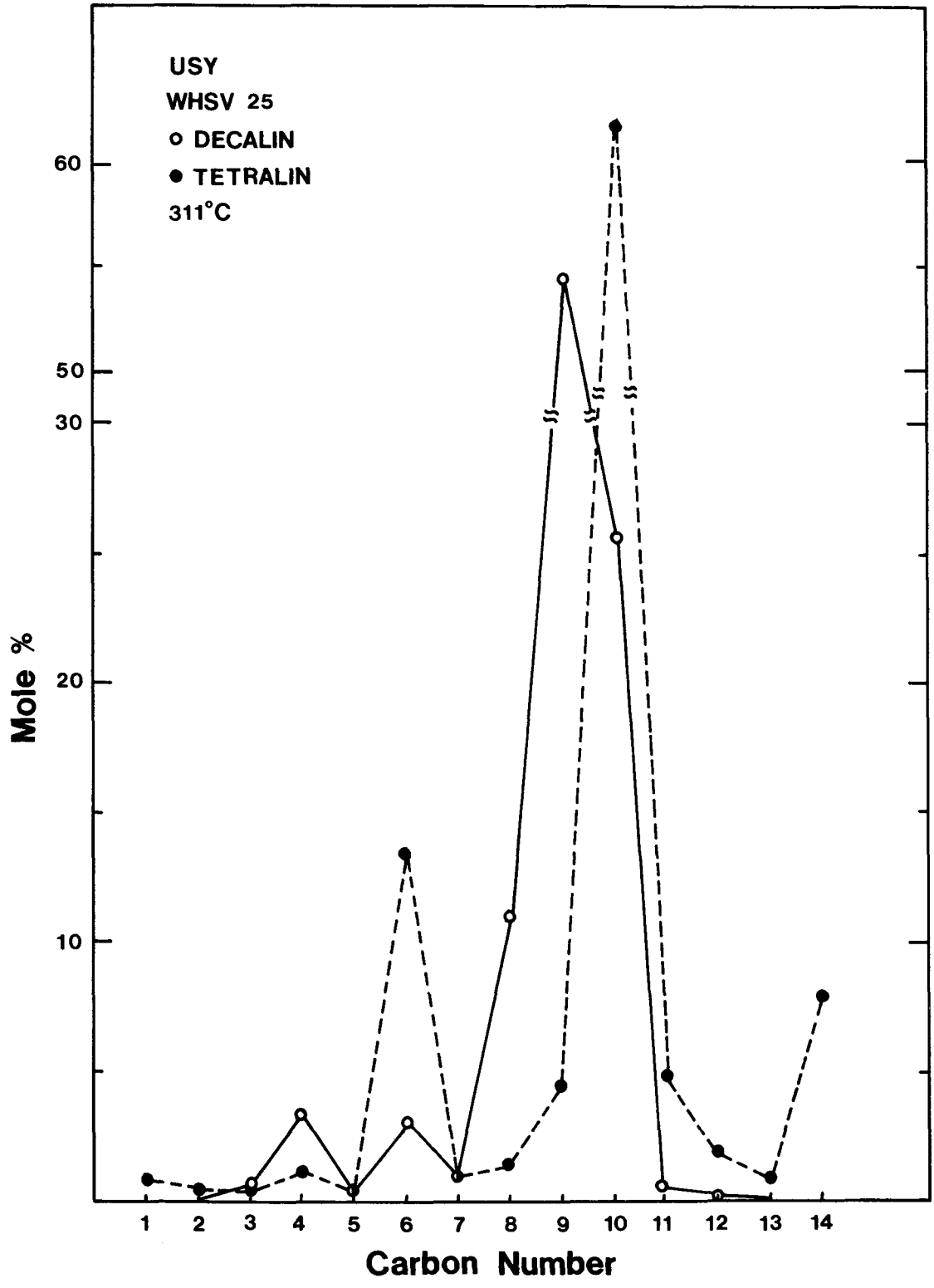

Fig. 7.18. Product Distribution over USY Zeolite. (40 Minutes Time-on-Stream, C_A° in Vol % Vapor at STP, 6.0% for Tetralin, 5.2% for Decalin).

Table 7.2

Product Distribution from Reaction of Decalin and Tetralin over USY Zeolite

Reactant		Decalin			Tetralin
Feed Rage, liquid		0.616 cc/hr			0.616 cc/hr
Catalyst Weight		0.024 g			0.24 g
Superficial Contact Time *1		1 second			1 second
Reaction Temperature		314°C			311°C
Total Conversion		49.79%			8.526%
Total Rate Constant *2		15.67			2.25
Time-on-Stream, min.		30			94
Wt% C on Catalyst		6.65%			8.45%
Mole% in Total Product					
Methane	C_1	-	C_1		0.8
Ethane + Ethene	C_2	-	C_2		0.4
Propane + Propene	C_3	0.6	C_3		0.2
Butane + Butenes	C_4	3.3	C_4		1.0
Cyclic	C_5	0.3	Cyclo-pentane	C_5	0.3
+	C_6	3.0	Benzene	C_6	0.5
Noncyclic	C_7	0.8	Cyclohexane		12.8
	C_8	11.0	Toluene	C_7	0.9
	C_9	54.7	Ethylbenzene Styrene	C_8	1.2
	C_{10}	22.2	Methyl-, ethyl-benzene propylbenzene	C_9	4.3
Hydro-naphthalenes Naphthalene	C_{10}	3.3	n-butyl, tert-butylbenzene	C_{10}	12.5
Methyl-tetralin naphthalene	C_{11}	0.6	Methylindans		13.0
Dimethyl-tetralin naphthalene	C_{12}	0.1	Naphthalene	C_{10}	36.2
			Two fused ring	C_{11}	4.9
				C_{12}	1.9
				C_{13}	1.0
			Unidentified	C_{14} +	8.0

*1 Defined as volume of catalyst (c.c.) divided by the total gas flow rate (STP, cc/sec).

*2 Defined as g/g-cat/hr.

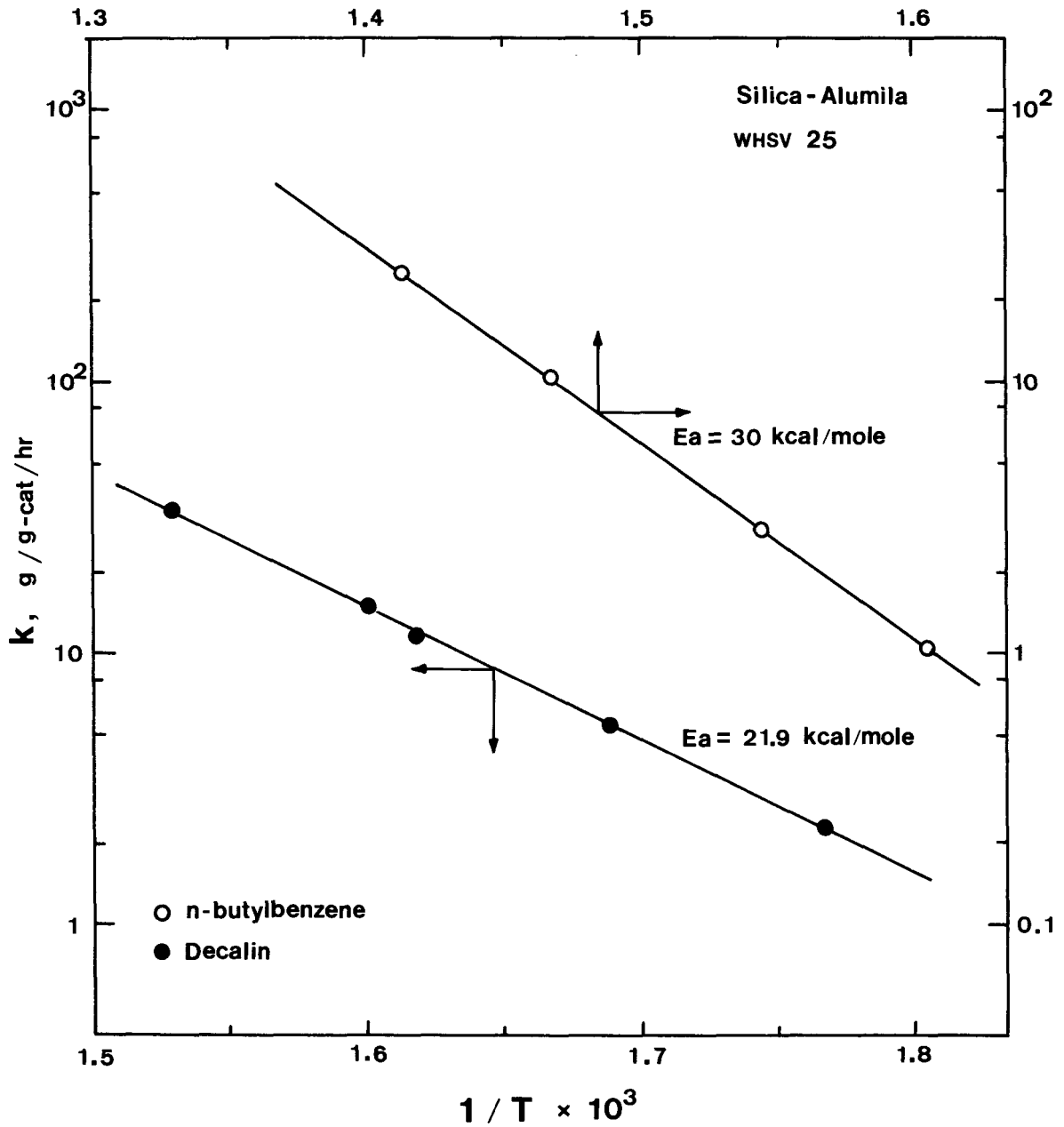

Fig. 7.19. Arrhenius Plot of First Order Rate Constant over Silica-Alumina.

will be in the neighborhood of 20 kcal/mole. Figure 7.20 presents the Arrhenius plot of decalin cracking over USY zeolite. Each activity measurement again is based on a reaction of 40 minutes time-on-stream. It is very clear that the reaction is diffusion limited when the reaction temperature is above 175°C. In such circumstance, the activation energy in a temperature above 200°C is reduced to about one half of the activation energy when the reaction is in kinetically controlled region which is in a temperature below 170°C. In our experiments, the catalyst particles are in 60-80 mesh size which is crushed from pelletized powder form USY zeolite. The mass transfer limitation observed over USY particles may be a combination of intercrystalline and macropore diffusion. Therefore, powder form USY zeolites which contains only distribution of the zeolite crystallite sizes is used to test for the possible contribution of macropore diffusion. The activities measured over powder form USY and over 60-80 mesh particles showed no significant differences, indicating that the diffusion of decalin in zeolite USY is primarily intracrystalline diffusion into zeolite crystallites. Therefore, the superactivity of USY zeolite will be limited by the diffusion of the reactants into zeolite crystallites.

An example of reaction of decalin over another acidic zeolite is shown in Figure 7.21. The catalyst employed in Figure 7.21 is a (62% La) LaNaY zeolite which is made by ion-exchanging NaY with Lanthanum ions. Each activity measurement is again based on a reaction of 40 minutes time-on-stream. The Arrhenius plot indicates that the catalytic cracking of decalin becomes diffusion limited when the reaction temperature is above 330°C. This temperature is higher than the limiting temperature when USY is used as catalyst because LaNaY is comparatively less active than USY. Figure 7.22 presents an additional example of decalin cracking over a (~60% La) LaHY zeolite. The LaHY zeolite is made by double-ion-exchange of the parent NaY zeolite. In chemical nature, the activity of LaHY for cracking lies between the activities of LaY and USY zeolites. Thus, it is expected that the reaction is found to be diffusion controlled when the reaction temperature is above 220°C.

Evaluation of Intracrystalline Diffusion Coefficient. We have shown that the performance of our flow microreactor can be described by a plug-flow assumption. For a typical first order diffusion limited reaction in a plug flow reactor, the total conversion can be correlated with the generalized Thiele modulus $\hat{h}p$ by the following expression,

$$\frac{W}{\dot{V}} = \hat{h}p \int_{C_A}^{C_A^\circ} \frac{d\,C_A}{k\,C_A}$$

$$= \hat{h}p \times \frac{1}{k} \ln \frac{1}{1-X_t} \qquad (10)$$

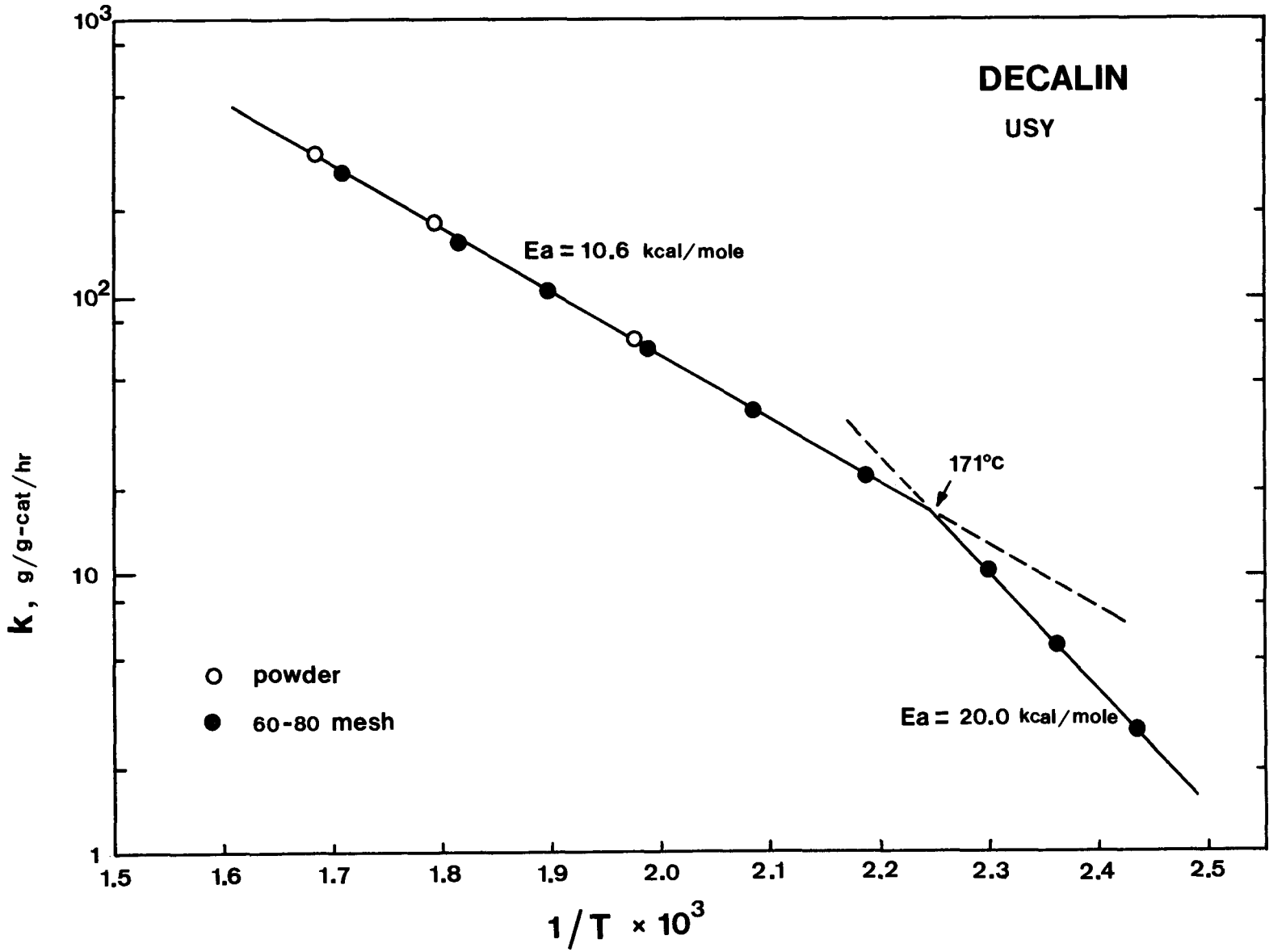

Fig. 7.20. Arrhenius Plot of First Order Rate Constant over USY Zeolite.

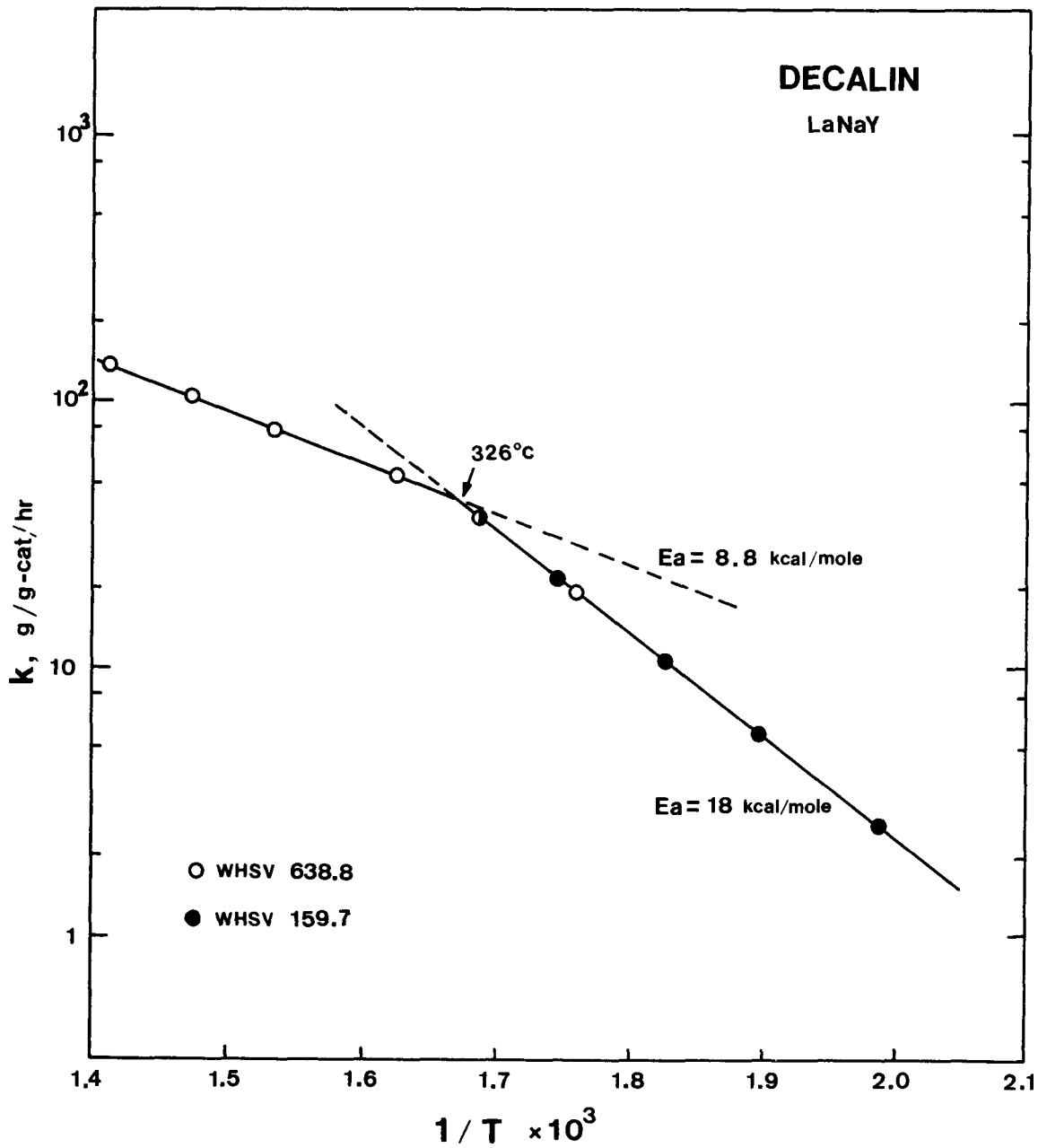

Fig. 7.21. Arrhenius Plot of First Order Rate Constant over LaNaY Zeolite.

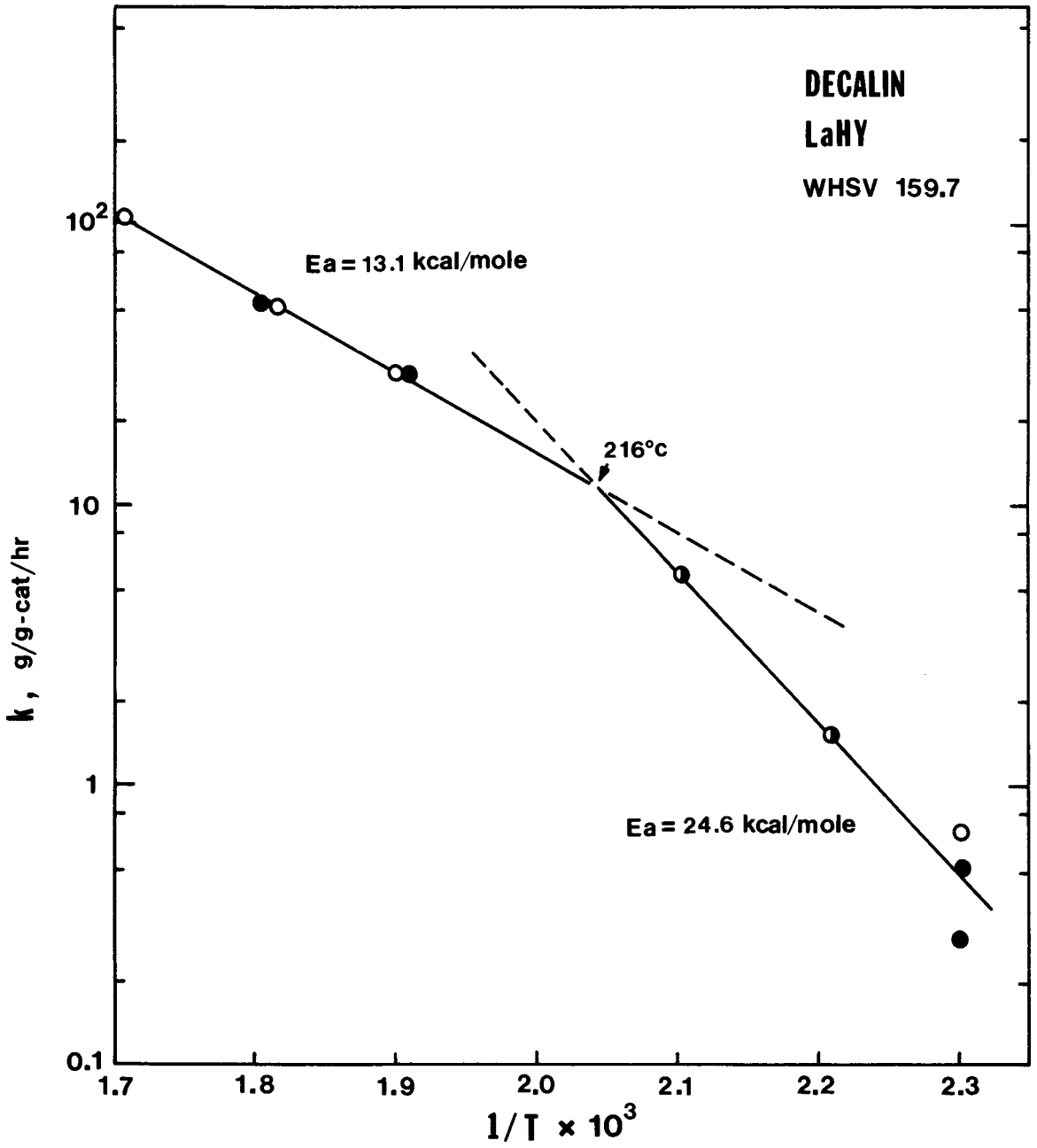

Fig. 7.22. Arrhenius Plot of First Order Rate Constant over LaHY Zeolite.

and

$$hp = \left(\frac{V_p}{A_p}\right) \sqrt{\frac{\rho \cdot k}{D}} \tag{11}$$

where V_p is the volume of catalyst particle, A_p its surface, ρ its density and D is the intercrystalline diffusion coefficient. The expression for reaction in the kinetically controlled region is

$$\frac{W}{\dot{V}} = \frac{1}{k} \ln \frac{1}{1-X_t} \tag{12}$$

Therefore, the hypothetical transition point from kinetic controlled region to diffusion limited region by extrapolating two slopes in Arrhenius plot is equivalent to a mathematical expression

$$\hat{hp} = 1 \tag{13}$$

Thus, an estimate of the intracrystalline diffusion coefficient can be evaluated at that particular temperature by the equation

$$D = \left(\frac{V_p}{A_p}\right)^2 \times \rho k \tag{14}$$

For simplicity, we assume the geometry of the particles to be spheres. With a distribution of sizes in i categories, the mean diameter d_m is expressed by

$$\left(\frac{V_p}{A_p}\right) = \frac{\Sigma v_i}{\Sigma a_i} = \frac{\Sigma 1/6\ \pi\ n_i d_i^3}{\Sigma\ \pi\ n_i d_i^2} = \frac{1}{6} \cdot \frac{\Sigma n_i d_i^3}{\Sigma n_i d_i^2} = \frac{1}{6} d_m \tag{15}$$

where v_i and a_i are the volume and surface area of each category. Equation (15) will also be valid for other geometries such as cubic and cylinder (length equals to diameter). The particle size distribution for our zeolite sample (LY2-52 powder, sodium acetate treated) was determined by a video microscopy technique (6). This particle size distribution can be best described by a logrithmic probability curve as shown in Figure 7.23. The dots are experimental points which averages over eight different measurements. The solid line is a theoretical size-frequency curve. The average diameters of different definitions shown in the right corner in Figure 7.23 are calculated from a method developed by Hatch and Choate (7). In that method, the size is completely defined by two parameter Mg (the geometric

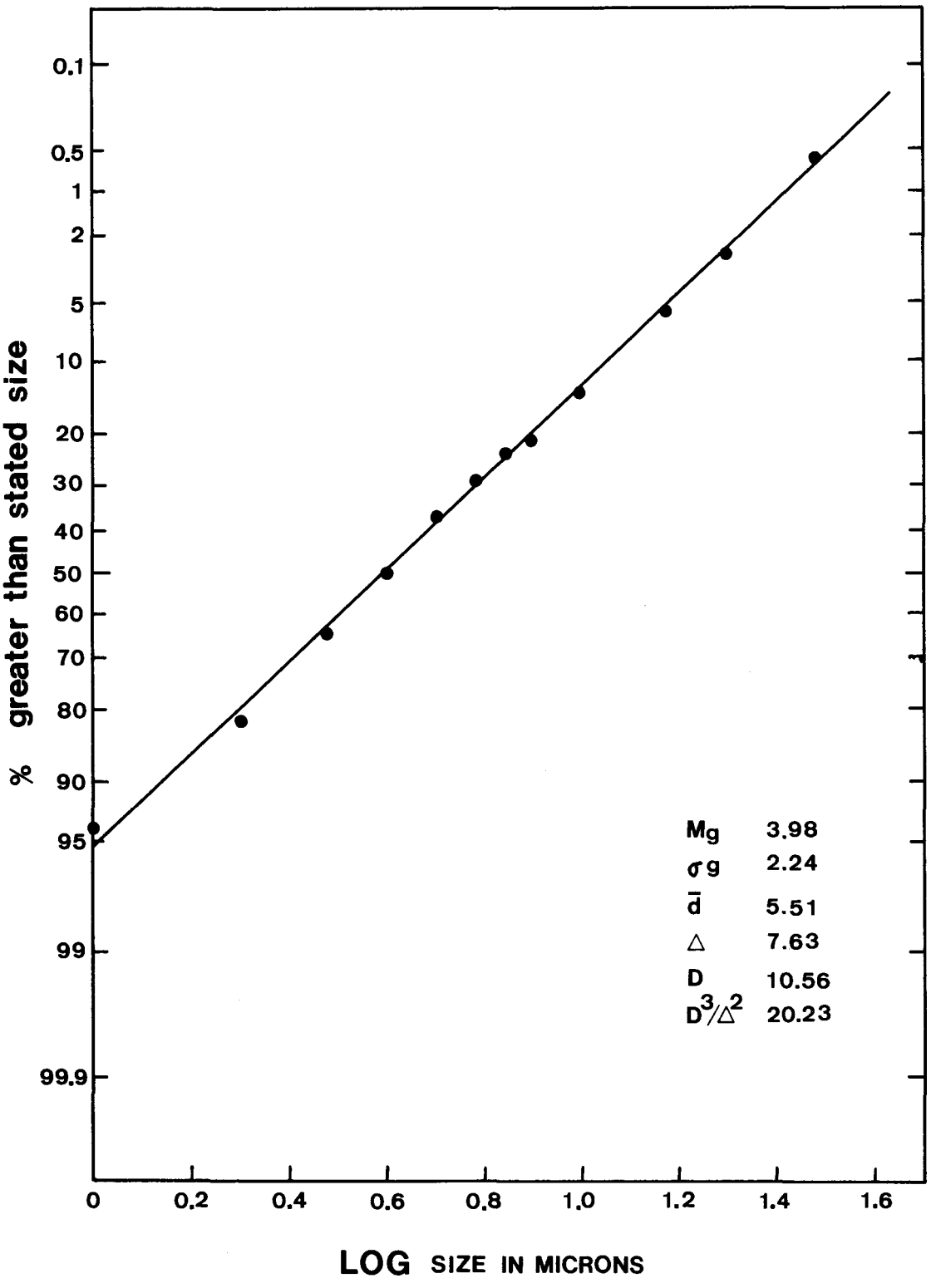

Fig. 7.23. Crystallite Size Distribution of NaY Zeolite.

mean) and σ_g (the geometric standard deviation) instead of a series of average diameters, thus simplifying the mathematical description. According to Hatch, average diameter d_m is

$$d_m = \frac{D^3}{\Delta^2} = \frac{\Sigma n_i d_i^3}{\Sigma n_i d_i^2} = \log Mg + 5.7565 \log^2 \sigma_g$$

$$= 20.23 \ \mu m \tag{16}$$

An additional problem in the evaluation of diffusion coefficient is the decay of the catalyst. One of the possible ways is find out the time independent activity. This may be done by curve fitting the experimental points with a best decay function and then extrapolating to zero time to obtain the initial activity. In Fig. 7.24, it shows that the decay function of decalin cracking over USY and LaNaY zeolites can be described quite well by a first order decay kinetics. Thus, initial rate constants can be easily evaluated. The deviation of the decay function at short period of time-on-stream (less than 30 minutes) may be due to unsteady state reaction. The density of catalyst particles is assumed to be equal to 1.0 g/cc. Now, we have all the information available for equation (14) and we can evaluate the intracrystalline diffusion coefficients.

Over NaY catalyst, the reaction is in kinetically controlled up to 630°C. Therefore,

$$D\ (630°C) > \left(\frac{V_p}{A_p}\right)^2 \times \rho k$$

or

$$D\ (630°C) > 2.38 \times 10^{-7} \ cm^2/sec \tag{17}$$

which gives a criterion of the order of magnitude of diffusion coefficient of deaclin into Y type zeolites.

Over LaNaY, the hypothetical transition temperature is 326°C. Thus,

$$D\ (326°C) = 2.30 \times 10^{-7} \ cm^2/sec \tag{18}$$

Over LaHY, the hypothetical transition temperature is 216°C. We obtain,

$$D\ (216°C) = 6.46 \times 10^{-8} \ cm^2/sec \tag{19}$$

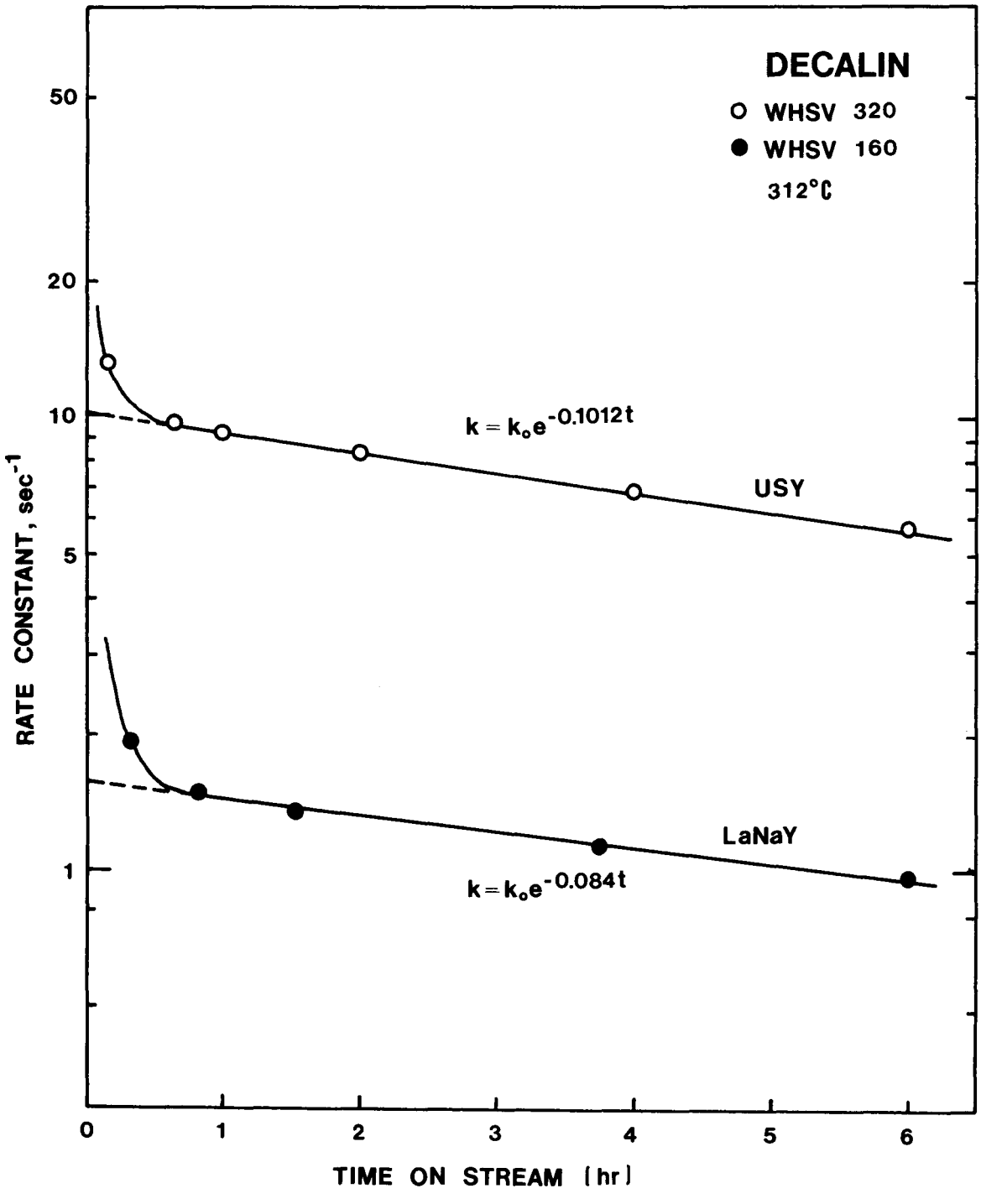

Fig. 7.24. Decay Function of First Order Rate Constant.

Over USY, the hypothetical transition temperature is 171°C. However, we have not measured the particle size distribution of USY crystallites yet. Estimation of mean diameter using the mean diameter obtained for NaY crystallite is temporarily employed for this comparison. We obtain

$$D\ (171°C) = 9.30 \times 10^{-8}\ cm^2/sec \qquad (20)$$

It is clear that the diffusion coefficient for decalin into Y type zeolites obtained from our experiments at a temperature of about 100°C to 300°C are in the order of 10^{-7} to 10^{-8} cm^2/sec. Unfortunately, very limited information on diffusion in Y-type zeolites is available for comparison with the results of our studies. Relevant data to our results were reported by three different groups, MacDonald, et al (8), Ruthven, et al (9) and Karger, et al (10). The former two groups estimated diffusivities of benzene, heptane and octane into 13X zeolite at a temperature of 130°C ~ 430°C were within the order of 10^{-9} cm^2/sec which is an order magnitude lower than our values. While the German group calculated diffusivities of hexane and heptane into NaX zeolite at a temperature of 100°C were within the order of 10^{-5} to 10^{-6} cm^2/sec which is about two order magnitudes higher than our results. Generally speaking, the free aperture of acidic Y-type zeolites is greater than that of 13X sieve. However, the size of hydrocarbon molecules we used (e.g. decalin) is significantly greater than that used by other researchers. Therefore, it will be very difficult to draw any conclusion at this time. We have also estimated the diffusional activation energy of decalin into acidic faujasites by making an Arrhenius plot of results over LaY and LaHY catalyst. A value of 6.7 kcal/mole is obtained. This value is pretty reasonable because the size of decalin is about 7 Å, which is less than the aperture of acidic faujasite that is about 8 Å. Therefore, the decalin molecules seem to have no great difficulty in entering the acidic faujasite crystallites. Hsu has found the rate of diffusion of decalin in zeolite NaY to be too rapid to evaluate by the chromatography technique. (See discussion under Task 1.)

Work Forecast:

In the next quarter, the catalytic cracking of fused-ring compounds with larger critical diameters such as 1-methyldecalin, 1-dimethyldecalin and perhydrophenanthrene over acidic Y-type zeolites will be analyzed. Intracrystalline diffusion coefficients of these compounds into acidic Y-type zeolites will be evaluated. Selectivities among the pore diffusion limiting reaction conditions and insignificant pore diffusion reaction conditions will be discussed.

Task 5 - Hydrocracking Studies on Zeolite Containing Catalysts - C. Chen T.M. Lai, and H.W. Haynes, Jr.

During the last quarter analysis of the data from Run CCC01 (hydrocracking of prehydrogenated phenanthrene) was completed. Unfortunately the carbon material balances were very poor and it was decided to scrap the data and repeat the run. Several reasons were set forth for the low material balances. A small leak was found in the feed pump seal. The packing was replaced. Also, it became apparant that poor technique was employed in depressuring the product accumulator at the run termination which would result in the loss of C_3-C_5 hydrocarbons. In subsequent runs a dry ice-acetone cold trap was installed in the vent upstream of the wet test meter and the pressure was reduced slowly over a period of from one to two hours. In this report we will discuss the preliminary results from hydrocracking a mixture of hydrogenated pyrenes over the NiWH-USY zeolite catalyst described in the previous report. Midway through the run the feed was switched to pure tetralin and data on tetralin hydrocracking were also obtained.

Catalyst

The zeolite catalyst was from the same batch described in the previous report. However, it was believed that the hydrogenated pyrenes might be more refractory than the hydrogenated phenanthrenes, so the zeolite fraction of the pilled catalyst was increased. For these experiments a 34.2770 g portion of the W-impregnated $NiNH_4$-USY zeolite powder was mixed with 94.7 g of Conoco Catapal SB (both weights after vacuum drying at 200°C for two hours) and the mixture was tabletted without a lubricant. The dry catalyst composition is provided in Table 7.3 below:

Table 7.3

Calculated Dry Catalyst Composition

Tun TML02

$(NH_4)_2WO_4$	2.91 wt%
$NiNH_4$-USY*	23.66 wt%
$Al_2O_3 \cdot H_2O$	73.42 wt%

*Ni^{++}/Al atom ratio = 0.042

NH_4/Al atom ratio = 0.260

Na^+/Al atom ratio = 0.01

The catalyst was ground and sieved to 10-20 mesh, calcined and sulfided according to the procedure discussed in the previous report.

Feed Preparation

Pure pyrene (Aldrich, 99^{+}%) was hydrogenated in a batch autoclave reactor in the presence of a nickel catalyst according to the procedure outlined in the earlier report. The hydrogenation was carried out at 300°C and 2000 psi. No carbon-carbon bond breakage was observed at these conditions. After each batch run the liquid was siphoned off and stored. Solids were mixed with fresh pyrene and reacted in the subsequent batch run. Analysis of the combined prehydrogenated pyrenes feed by GC/MS revealed the composition of Table 7.4. The tetralin feed was Aldrich, 99% purity. Both feeds were spiked with CS_2 to give one weigh percent sulfur in the feed.

Table 7.4

Feed Analysis by Gas Chromatography

Compound	Retention* Time, min	Weight Percent
Unknown	11.63	0.2
Unknown	39.75	0.4
Unknown	40.33	0.2
Unknown	40.99	0.4
Unknown	43.41	0.3
Perhydropyrene	44.56	17.8
Perhydropyrene	45.82	12.1
Perhydropyrene	46.64	6.4
Unknown	47.98	1.2
Decahydropyrene	49.05	7.0
Decahydropyrene	50.17	39.9
Unknown	51.33	0.9
Unknown	52.12	0.6
Hexahydropyrene	53.72	4.5
Hexahydropyrene	54.88	7.7
Dihydropyrene	56.27	0.4
Pyrene	59.63	0.1
		100.1

*See Table 7.5 for GC conditions.

Results

The products from a yield period consisted of a gas sample, a liquid

Table 7.5

GC Column Conditions

	Liquid	Gas
Column	1/8" (0.069"I.D.) × 4m S.S. tubing packed with 10% SE-30 on 80/100 Mesh Chromosorb W-HP	1/8" (0.069"I.D.) × 6 ft. Chromosorb 102, 80/100 mesh
Carrier Gas	Nitrogen, 10 cc/min	Nitrogen, 20 cc/min
Injection Temperature	250°C	-
FID Temperature	275°C	250°C
Column Program	30-250°C at 5°C/ min. Isothermal at 250°C for 10 min	120-150°C at 5°C/ min. Isothermal at 150°C for 10 min
Sample Size	1 microliter	~0.1 ml sample loop
Sample Dilution	20/1 or 100/1 in CS_2	-

(mostly C_3-C_5) sample from the cold trap and a liquid sample from the high pressure accumulator. The gas sample was analyzed immediately after the completion of a yield period by gas chromatography. The two liquid samples were combined, capped, and stored in a freezer for later analysis. Portions of the liquid sample were diluted with cold carbon disulfide for analysis by gas chromatography. When solids were present the entire sample was diluted until all solids were dissolved. Gas chromatography conditions are listed in Table 7.5. An example chromatogram is provided in Fig. 7.25.

A preliminary partial computer printout of the results from Run TML02 is listed in the appendix. The first thing to point out is the carbon material balance. In yield periods 1-7 (hydrogenated pyrenes feed) the material balances were less than satisfactory. Occasional temporary plugging of the lines was experienced throughout this series of runs and there was evidence of a build-up of solids on the wall of the accumulator. The material balances for the tetralin yield periods were much improved and operation of the equipment was much smoother. In all these results the yields have been corrected to force a 100% carbon material balance.

A detailed analysis of these results is in progress and will not be reported at this time. However, it is clear that the zeolite catalyst is very active for the conversion of the prehydrogenated pyrenes and tetralin. In some cases the feed is converted almost totally to C_3-C_5 hydrocarbons. The catalyst does deactivate although the activity remained high at the end of the run after 170 hours on stream. It is emphasized that these results are preliminary and subject to refinement.

Work Forecast:

The analysis of these data will continue during the next quarter. The hydrocracking kinetics will be evaluated for both hydrogenated pyrenes and tetralin. A similar series of experiments is planned for a feed consisting of hydrogenated phenanthrenes. A capillary column will be installed on the GC to try and improve the resolution of the components of the liquid product sample.

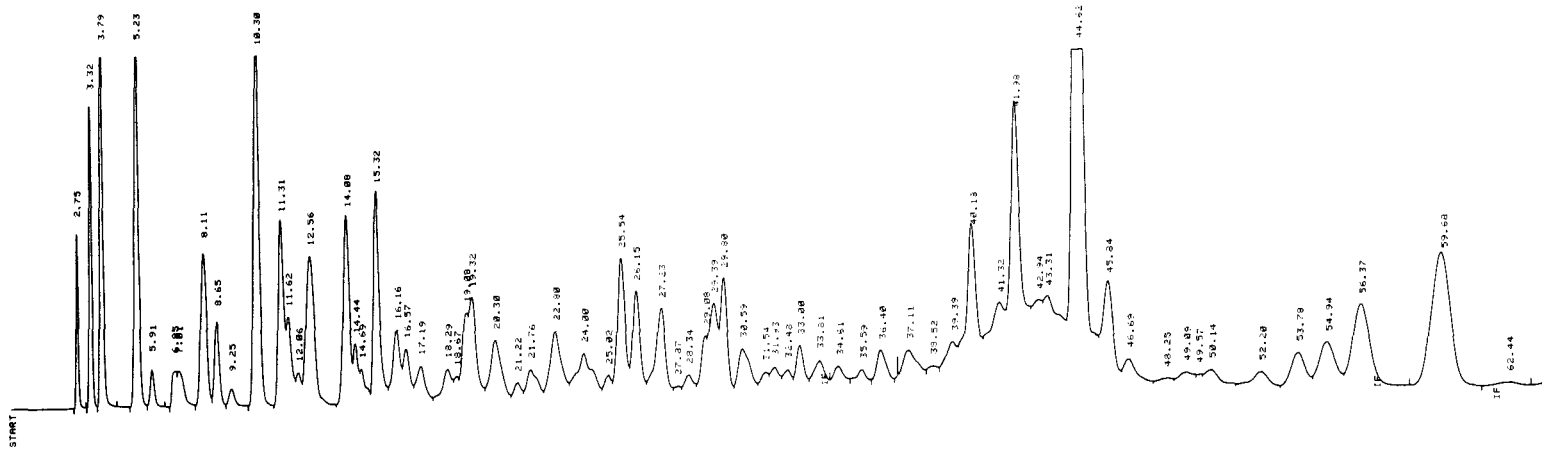

Fig. 7.25. Example Gas Chromatogram. Liquid Product from Run TML02-5. Some Representative Retention Times: Propane = 2.75, Isopentane = 5.23, Solvent (CS_2) = 7.01, Methylcyclopentane = 10.30, Methylcyclohexane = 15.32, Indan = 25.54, Tetralin = 25.80, Perhydropyrene = 44.62, Hexahydropyrene = 53.78, Dihydropyrene = 56.37, Pyrene = 59.68.

References

1. Cerro, R. L. and Smith, J. M., Jud. Eng. Chem., Fund. 8, 796 (1969).

2. Ruthven, D. M., ACS Symp. Ser. 40, 320 (1977).

3. Quarterly Report No. FE-2727-5 for Period October 1 - December 31, 1978, dated February 12, 1978.

4. Quarterly Report No. FE-2727-6 for the Period January 1 - March 31, 1979, dated May 14, 1979.

5. Nace, D. M., Ind. Eng. Chem., Prod. Res. Dev., 8, 24 (1969).

6. Analyzed by Dr. M. P. Mathur,Pittsburgh Energy Research Center, Department of Energy.

7. Hatch, T. and Choate, S. P., Journal Franklin Institute, March 1929, P. 369.

8. MacDonald, W. R. and Habwood, H. W., Can. J. Chem. Eng., 50, 462 (1972).

9. Ruthven, D. M. and Doetsch, I. H., A.I.Ch.E.J., 22, 882 (1976).

10. Karger, J., Shadanov, S. P. and Walter A., Z. Phys. Chem. (Leipzig), 256 319 (1975).

RUN TIL02, 5.746 GMS 25% (APPROX) NIHHUSY ZEOLITE, HYDROGENATED PYRENES FEED
RUN SUMMARY

YIELD PERIOD NO.	1.	2.	3.	4.	5.	6.
YIELD PERIOD LENGTH, HRS.	10.166	4.933	5.000	2.717	6.500	6.000
TEMPERATURE, F	702.0	708.0	654.0	705.0	742.0	810.0
PRESSURE, PSIG	1530.	1510.	1535.	1500.	1510.	1520.
LIQUID FEED RATE, CC/HR	3.1	6.1	6.1	12.4	6.2	6.2
LIQUID SPACE VELOCITY, GM/HR/GM	0.550	1.082	1.094	2.213	1.101	1.100
SPACE TIME, (GM/HR/GM)-1	1.817	0.925	0.914	0.452	0.908	0.909
APPROX. H2 TREAT RATE, L(STP)/HR	10.0	10.0	10.0	15.0	10.0	10.0
APPROX. H2 TREAT RATE, L(STP)/GM	3.163	1.609	1.591	1.180	1.580	1.582
EXIT GAS RATE, L(STP)/HR	10.0	11.3	8.4	10.4	7.4	8.3
CUMULATIVE HRS ON CATALYST	17.42	32.47	41.86	50.72	61.11	72.86
CUMULATIVE GMS OIL/GM CATALYST	11.44	24.54	34.91	48.35	62.09	73.98
LIQUID MATERIAL BALANCE, WT%	55.4	68.4	107.1	72.9	82.5	68.2
CARBON MATERIAL BALANCE, WT%	84.5	78.5	117.1	77.6	92.8	92.6

CORRECTED YIELDS BASED ON LIQUID FEED

CONVERSION TO C15-, MOLE%	98.413	64.562	36.143	36.739	72.856	96.679
HYDROGEN CONSUMPTION, L(STP)/GM	0.964	0.201	0.110	0.003	0.192	0.918
HYDROGEN CONSUMPTION, WT%	6.667	1.805	0.994	0.027	1.723	8.257
GAS YIELD (C1-C4), WT%	82.661	16.185	9.769	5.419	15.893	77.244
NAPHTHA YIELD (C5-C11), WT%	24.409	32.217	15.941	17.575	42.777	27.173
LIQUID YIELD (C5+), WT%	26.006	85.620	91.225	94.608	85.831	31.013
C5-C8 YIELD, MOLE%	67.511	49.987	23.713	23.149	65.177	67.152
C9-C12 YIELD, MOLE%	0.251	30.609	17.329	21.891	35.316	2.778
C13+ YIELD, MOLE%	1.587	47.276	70.981	72.667	38.454	3.748

RUN THL02, 5.746 GMS 25% (APPROX) NIWHUSY ZEOLITE, HYDROGENATED PYRENES FEED
RUN SUMMARY

YIELD PERIOD NO.	7.
YIELD PERIOD LENGTH, HRS.	13.934
TEMPERATURE, F	707.0
PRESSURE, PSIG	1520.
LIQUID FEED RATE, CC/HR	3.1
LIQUID SPACE VELOCITY, GM/HR/GM	0.550
SPACE TIME, (GM/HR/GM)-1	1.817
APPROX. H2 TREAT RATE, L(STP)/HR	10.0
APPROX. H2 TREAT RATE, L(STP)/GM	3.163
EXIT GAS RATE, L(STP)/HR	9.6
CUMULATIVE HRS ON CATALYST	90.33
CUMULATIVE GMS OIL/GM CATALYST	85.10
LIQUID MATERIAL BALANCE, WT%	67.2
CARBON MATERIAL BALANCE, WT%	88.4

CORRECTED YIELDS BASED ON LIQUID FEED

CONVERSION TO C15-, MOLE%	67.954
HYDROGEN CONSUMPTION, L(STP)/GM	0.409
HYDROGEN CONSUMPTION, WT%	3.678
GAS YIELD (C1-C4), WT%	28.809
NAPHTHA YIELD (C5-C11), WT%	31.274
LIQUID YIELD (C5+), WT%	74.869
C5-C8 YIELD, MOLE%	61.548
C9-C12 YIELD, MOLE%	17.842
C13+ YIELD, MOLE%	39.186

RUN TEL02, 5.746 GMS 25% (APPROX) NIWHUSY ZEOLITE, TETRALIN FEED
RUN SUMMARY

YIELD PERIOD NO.	8.	9.	10.	11.	12.	13.
YIELD PERIOD LENGTH, HRS.	13.217	4.000	9.750	3.500	3.500	11.000
TEMPERATURE, F	701.0	698.0	700.0	773.0	655.0	712.0
PRESSURE, PSIG	1510.	1500.	1515.	1520.	1520.	1520.
LIQUID FEED RATE, CC/HR	3.1	12.6	6.2	12.3	12.3	3.1
LIQUID SPACE VELOCITY, GM/HR/GM	0.514	2.099	1.029	2.055	2.059	0.515
SPACE TIME, (GM/HR/GM)-1	1.945	0.476	0.972	0.487	0.486	1.942
APPROX. H2 TREAT RATE, L(STP)/HR	10.0	12.0	10.0	15.0	13.0	10.0
APPROX. H2 TREAT RATE, L(STP)/GM	3.385	0.995	1.692	1.270	1.099	3.381
EXIT GAS RATE, L(STP)/HR	9.9	13.1	12.6	12.6	16.7	10.8
CUMULATIVE HRS ON CATALYST	114.11	126.08	136.38	148.25	155.00	169.50
CUMULATIVE GMS OIL/GM CATALYST	92.90	107.13	119.40	137.99	151.89	162.15
LIQUID MATERIAL BALANCE, WT%	68.6	96.2	93.2	92.5	97.0	85.8
CARBON MATERIAL BALANCE, WT%	102.7	98.6	96.8	97.8	97.6	100.3

CORRECTED YIELDS BASED ON LIQUID FEED

CONVERSION TO C 9-, MOLE%	99.219	38.467	55.895	98.061	14.159	95.762
HYDROGEN CONSUMPTION, L(STP)/GM	0.945	0.125	0.190	0.581	0.050	0.675
HYDROGEN CONSUMPTION, WT%	8.497	1.124	1.705	5.222	0.446	6.073
GAS YIELD (C1-C4), WT%	68.696	5.402	9.890	33.352	1.808	38.187
NAPHTHA YIELD (C5-C11), WT%	35.405	87.750	86.680	70.520	95.692	67.394
LIQUID YIELD (C5+), WT%	39.801	95.722	91.815	71.871	98.638	67.887
C5-C8 YIELD, MOLE%	55.421	22.601	37.882	103.288	9.382	97.781
C9-C12 YIELD, MOLE%	1.764	75.070	64.449	4.584	91.131	5.369
C13+ YIELD, MOLE%	2.662	3.709	2.238	0.648	0.926	0.285

RUN TLL02, 5.74G GMS 25% (APPROX) NIWHUSY ZEOLITE, HYDROGENATED PYRENES FEED

CORRECTED PRODUCT YIELDS BASED ON LIQUID FEED, WT%

YIELD PERIOD NO.		1.	2.	3.	4.	5.	6.
C 1H 4	METHANE	0.686	0.199	0.081	0.130	0.227	1.585
C 2H 6	ETHANE	4.697	0.778	0.123	0.251	1.027	6.547
C 3H 8	PROPANE	30.732	6.911	1.224	2.490	6.547	34.644
C 4H10	I-BUTANE	27.720	4.666	7.684	1.408	3.499	17.009
C 4H10	N-BUTANE	18.827	3.630	0.656	1.138	4.592	17.460
C 5H12	I-PENTANE	10.166	3.457	1.194	1.403	3.527	8.252
C 5H12	N-PENTANE	5.122	0.246	0.054	0.027	0.287	3.081
C 6H14		1.310	1.058	0.446	0.371	1.509	1.756
C 6H14		0.610	0.464	0.208	0.167	0.697	0.815
C 6H14	N-HEXANE	0.554	0.092	0.041	0.032	0.162	0.495
C 6H12	METHYLCYCLOPENTANE	0.434	2.667	1.149	1.129	3.458	1.539
C 6H 6	BENZENE	0.000	0.000	0.000	0.235	1.618	0.000
C 6H12	CYCLOHEXANE	4.782	2.272	0.981	0.419	0.874	2.788
C 6H12		0.000	0.201	0.107	0.091	0.293	0.179
C 7H14		0.116	1.520	0.771	0.739	2.118	0.820
C 7H14	DIMETHYLCYCLOPENTANE	0.066	1.486	0.824	0.789	1.846	0.506
C 7H14		0.021	0.312	0.153	0.170	0.505	0.190
C 7H14		0.000	0.316	0.213	0.177	0.366	0.000
C 7H14		0.000	0.000	0.000	0.000	0.000	0.000
C 7H14	METHYLCYCLOHEXANE	0.555	0.867	0.339	0.469	2.151	3.005
C 7H 8	TOLUENE	0.038	0.861	0.635	0.516	0.961	0.103
C 7H 8		0.023	0.528	0.341	0.318	0.669	0.048
C 7H 8		0.027	0.548	0.355	0.357	0.649	0.044
C 7H 8		0.005	0.471	0.316	0.313	0.578	0.029
C 7H 8		0.000	0.212	0.135	0.133	0.227	0.001
C 7H 8		0.000	0.000	0.287	0.000	0.848	0.000
C 8H10	DIMETHYLBENZENE	0.319	1.318	0.398	0.789	1.446	1.493
C 8H10	O-XYLENE	0.123	0.954	0.601	0.604	1.259	0.479
C 8H10		0.000	0.230	0.141	0.158	0.297	0.012
C 8H10		0.000	0.488	0.126	0.320	0.685	0.044
C 8H10		0.000	0.000	0.114	0.000	0.000	0.000
C 9H12	ISOPROPYLBENZENE	0.000	0.999	0.462	0.630	1.487	0.386
C 9H12		0.050	0.000	0.000	0.000	0.000	0.056
C 9H12		0.057	1.148	0.573	0.489	1.516	0.254
C 9H12		0.000	0.000	0.000	0.292	0.000	0.000
C 9H12		0.007	0.294	0.142	0.201	0.364	0.027
C 9H10	INDAN	0.000	1.259	0.468	0.770	1.811	0.107
C10H14	ISOBUTYLBENZENE	0.005	0.952	0.368	0.585	1.544	0.112
C10H14		0.000	0.000	0.000	0.000	0.000	0.000
C10H12	1-METHYLINDAN	0.004	1.301	0.535	0.835	1.827	0.102
C10H12		0.000	0.132	0.066	0.094	0.175	0.001
C10H12		0.005	0.442	0.253	0.296	0.482	0.022
C10H12		0.000	0.000	0.000	0.315	0.686	0.000
C10H12		0.005	1.289	0.544	0.502	1.271	0.168
C10H12	TETRALIN	0.006	1.882	0.909	1.232	1.587	0.074
C11H14	DIMETHYLINDAN	0.000	0.729	0.439	0.574	1.144	0.077
C11H14		0.000	0.254	0.401	0.216	0.302	0.004
C11H14		0.000	0.211	0.000	0.185	0.391	0.022
C11H14		0.000	0.156	0.218	0.145	0.286	0.019
C11H14	6-METHYLTETRALIN	0.001	0.396	0.367	0.311	0.523	0.037
C11H14	DIMETHYLINDAN	0.000	0.205	0.268	0.178	0.352	0.027
C12H16	6-ETHYLTETRALIN	0.001	0.179	0.206	0.116	0.181	0.016
C12H16		0.000	0.144	0.126	0.082	0.130	0.004
C12H16		0.001	0.583	0.373	0.445	0.453	0.025
C12H16		0.000	0.778	0.402	0.581	0.736	0.030

C12H16		0.000	0.263	0.192	0.253	0.243	0.000
C12H16		0.000	0.764	2.967	0.582	0.707	0.000
C12H16		0.003	3.664	0.000	2.898	2.762	0.093
C12H16		0.000	2.194	1.414	1.812	1.853	0.022
C13H12	4,5-BENZINDANE	0.000	4.069	1.748	3.011	5.042	0.279
C13H12		0.000	0.000	0.000	0.000	1.380	0.010
C13H12		0.000	3.868	2.548	3.003	2.379	0.036
C13H12		0.000	1.249	1.251	1.317	0.000	0.000
C16H26	PERHYDROPYRENE	0.477	18.416	30.405	24.305	15.214	1.996
C16H26	PERHYDROPYRENE	0.249	3.628	6.310	6.147	1.838	0.200
C16H26		0.097	1.087	1.783	1.924	0.479	0.022
C16H26		0.008	0.181	0.000	0.434	0.091	0.016
C16H20	DECAHYDROPYRENE	0.097	0.957	4.061	2.203	0.247	0.026
C16H20	DECAHYDROPYRENE	0.408	1.147	5.199	2.946	0.083	0.033
C16H20		0.000	0.000	0.225	0.000	0.328	0.000
C16H14	TETRAHYDROPYRENE	0.003	0.690	0.551	1.717	0.354	0.013
C16H16	HEXAHYDROPYRENE	0.088	1.982	4.255	4.436	0.777	0.054
C16H16	HEXAHYDROPYRENE	0.131	3.055	6.491	6.308	1.147	0.058
C16H12	DIHYDROPYRENE	0.021	2.703	2.162	5.345	2.331	0.126
C16H10	PYRENE	0.014	1.654	2.546	7.087	4.181	0.767
C17H12		0.000	0.127	0.068	0.082	0.116	0.013
TOTALS		108.667	101.805	100.994	100.027	101.723	108.257

RUN THL62, 5.746 GMS 25% (APPROX) NIWHUSY ZEOLITE, HYDROGENATED PYRENES FEED

CORRECTED PRODUCT YIELDS BASED ON LIQUID FEED, WT%

YIELD PERIOD NO.		7.
C 1H 4	METHANE	2.644
C 2H 6	ETHANE	3.268
C 3H 8	PROPANE	11.147
C 4H10	I-BUTANE	6.640
C 4H10	N-BUTANE	5.110
C 5H12	I-PENTANE	4.689
C 5H12	N-PENTANE	0.377
C 6H14		1.576
C 6H14		0.690
C 6H14	N-HEXANE	0.263
C 6H12	METHYLCYCLOPENTANE	2.944
C 6H 6	BENZENE	0.451
C 6H12	CYCLOHEXANE	2.192
C 6H12		0.313
C 7H14		1.621
C 7H14	DIMETHYLCYCLOPENTANE	1.924
C 7H14		0.892
C 7H14		0.000
C 7H14		0.000
C 7H14	METHYLCYCLOHEXANE	1.813
C 7H 8	TOLUENE	0.676
C 7H 8		0.461
C 7H 8		1.617
C 7H 8		0.218
C 7H 8		0.048
C 7H 8		0.000
C 8H10	DIMETHYLBENZENE	1.432
C 8H10	O-XYLENE	0.607
C 8H10		0.063
C 8H10		0.137
C 8H10		0.000
C 9H12	ISOPROPYLBENZENE	0.548
C 9H12		0.000
C 9H12		0.449
C 9H12		0.000
C 9H12		0.067
C 9H10	INDAN	0.721
C10H14	ISOBUTYLBENZENE	0.533
C10H14		0.000
C10H12	1-METHYLINDAN	0.593
C10H12		0.000
C10H12		0.128
C10H12		0.000
C10H12		0.658
C10H12	TETRALIN	0.646
C11H14	DIMETHYLINDAN	0.418
C11H14		0.000
C11H14		0.838
C11H14		0.118
C11H14	6-METHYLTETRALIN	0.262
C11H14	DIMETHYLINDAN	0.271
C12H16	6-ETHYLTETRALIN	0.338
C12H16		0.203
C12H16		0.523
C12H16		0.399

C12H16		0.468
C12H16		0.576
C12H16		2.245
C12H16		1.009
C13H12	4,5-BENZINDANE	2.325
C13H12		0.000
C13H12		1.877
C13H12		1.412
C16H26	PERHYDROPYRENE	15.054
C16H26	PERHYDROPYRENE	5.446
C16H26		1.695
C16H26		0.461
C16H20	DECAHYDROPYRENE	1.496
C16H20	DECAHYDROPYRENE	1.445
C16H20		0.000
C16H14	TETRAHYDROPYRENE	0.906
C16H16	HEXAHYDROPYRENE	1.370
C16H16	HEXAHYDROPYRENE	1.751
C16H12	DIHYDROPYRENE	1.431
C16H10	PYRENE	1.166
C17H12		0.000
TOTALS		103.678

RUN THL02, 5.746 GMS 25% (APPROX) NIWHUSY ZEOLITE, TETRALIN FEED

CORRECTED PRODUCT YIELDS BASED ON LIQUID FEED, WT%

YIELD PERIOD NO.		8.	9.	10.	11.	12.	13.
C 1H 4	METHANE	0.573	0.375	0.356	0.493	0.380	0.348
C 2H 6	ETHANE	2.854	0.189	0.257	1.193	0.099	1.033
C 3H 8	PROPANE	18.484	1.154	2.010	7.024	0.265	7.556
C 4H10	I-BUTANE	25.917	1.561	2.918	10.624	0.397	15.809
C 4H10	N-BUTANE	20.867	2.123	4.350	14.017	0.668	13.440
C 5H12	I-PENTANE	10.978	1.279	1.697	6.324	0.347	8.283
C 5H12	N-PENTANE	4.095	0.375	0.215	0.846	0.037	0.996
C 6H14		2.551	0.601	0.696	2.980	0.219	4.326
C 6H14		1.005	0.256	0.285	1.237	0.086	1.848
C 6H14	N-HEXANE	0.872	0.177	0.099	0.374	0.028	0.567
C 6H12	METHYLCYCLOPENTANE	0.904	1.014	2.334	6.733	0.513	10.333
C 6H 6	BENZENE	4.968	5.166	9.233	22.839	2.651	17.037
C 6H12	CYCLOHEXANE	0.000	0.000	0.000	0.000	0.000	0.000
C 6H12		0.145	0.119	0.215	0.668	0.000	0.731
C 7H14		0.417	0.596	1.222	2.854	0.264	3.156
C 7H14	DIMETHYLCYCLOPENTANE	0.247	0.494	1.038	1.769	0.213	2.163
C 7H14		0.074	0.211	0.432	0.650	0.060	0.724
C 7H14		0.000	0.000	0.000	0.000	0.000	0.036
C 7H14		0.000	0.000	0.000	0.032	0.000	0.000
C 7H14	METHYLCYCLOHEXANE	4.875	2.145	2.731	11.678	0.850	7.526
C 7H 8	TOLUENE	0.116	0.254	0.435	0.406	0.053	0.362
C 7H 8		0.052	0.153	0.269	0.215	0.021	0.215
C 7H 8		0.000	0.135	0.221	0.000	0.001	0.000
C 7H 8		0.020	0.094	0.225	0.096	0.036	0.133
C 7H 8		0.000	0.000	0.000	0.000	0.000	0.133
C 7H 8		0.000	0.447	1.630	3.301	0.455	1.354
C 8H10	DIMETHYLBENZENE	1.948	0.573	0.000	2.411	0.000	1.644
C 8H10	O-XYLENE	0.559	0.230	0.482	0.867	0.088	0.559
C 8H10		0.000	0.015	0.214	0.085	0.000	0.003
C 8H10		0.000	0.000	0.000	0.000	0.069	0.000
C 8H10		0.000	0.200	0.747	0.005	0.000	0.003
C 9H12	ISOPROPYLBENZENE	0.375	0.806	2.079	1.361	0.346	0.527
C 9H12		0.000	0.202	0.590	0.296	0.000	0.101
C 9H12		0.064	1.653	4.048	0.277	0.692	0.178
C 9H12		0.208	0.846	1.732	0.064	0.371	0.000
C 9H12		0.032	1.100	2.194	0.063	0.832	0.052
C 9H10	INDAN	0.048	1.509	2.679	0.000	0.591	0.031
C10H14	ISOBUTYLBENZENE	0.142	7.279	11.938	0.775	2.739	0.246
C10H14		0.000	0.000	0.000	0.000	1.886	0.104
C10H12	1-METHYLINDAN	0.176	13.390	12.709	0.432	4.910	0.279
C10H12		0.000	0.000	0.000	0.000	0.000	0.000
C10H12		0.015	0.597	0.733	0.012	0.954	0.041
C10H12		0.000	0.000	0.000	0.000	0.000	0.000
C10H12		0.000	0.000	0.000	0.000	1.936	0.000
C10H12	TETRALIN	0.451	40.374	18.903	0.732	73.483	3.573
C11H14	DIMETHYLINDAN	0.035	3.608	2.422	0.076	0.227	0.106
C11H14		0.000	0.501	0.366	0.000	0.000	0.002
C11H14		0.012	0.000	0.310	0.035	0.000	0.000
C11H14		0.000	0.043	0.166	0.000	0.187	0.000
C11H14	6-METHYLTETRALIN	0.000	0.847	0.000	0.023	0.397	0.020
C11H14	DIMETHYLINDAN	0.018	0.463	1.390	0.006	0.149	0.004
C12H16	6-ETHYLTETRALIN	0.011	0.133	0.180	0.017	0.013	0.004
C12H16		0.004	0.223	0.231	0.002	0.097	0.003
C12H16		0.016	0.140	0.027	0.010	0.103	0.002
C12H16		0.014	0.280	0.426	0.000	0.127	0.000

C12H16		0.000	0.396	0.346	0.044	0.274	0.002
C12H16		0.009	0.208	0.099	0.054	0.155	0.002
C12H16		0.094	0.754	0.401	0.009	0.267	0.000
C12H16		0.000	0.101	0.025	0.169	0.534	0.029
C13H12	4,5-BENZINDANE	0.149	0.666	0.274	0.000	0.493	0.000
C13H12		0.034	0.000	0.000	0.038	0.000	0.053
C13H12		0.000	0.132	0.024	0.000	0.009	0.000
C13H12		0.000	0.000	0.000	0.000	0.000	0.000
C16H26	PERHYDROPYRENE	1.893	2.543	0.413	0.270	0.355	0.092
C16H26	PERHYDROPYRENE	0.441	0.211	0.028	0.358	0.336	0.183
C16H26		0.088	0.068	0.010	0.048	0.000	0.000
C16H26		0.039	0.008	0.013	0.129	0.084	0.069
C16H20	DECAHYDROPYRENE	0.151	0.027	0.004	0.000	0.000	0.000
C16H20	DECAHYDROPYRENE	0.253	0.055	0.012	0.000	0.012	0.013
C16H20		0.000	0.000	0.001	0.023	0.014	0.000
C16H14	TETRAHYDROPYRENE	0.021	0.006	0.002	0.000	0.000	0.000
C16H16	HEXAHYDROPYRENE	0.158	0.067	0.014	0.032	0.013	0.011
C16H16	HEXAHYDROPYRENE	0.207	0.090	0.007	0.015	0.011	0.003
C16H12	DIHYDROPYRENE	0.169	0.233	0.000	0.015	0.014	0.008
C16H10	PYRENE	0.646	1.585	2.598	0.118	0.011	0.020
C17H12		0.000	0.046	0.000	0.000	0.024	0.000
TOTALS		108.497	101.124	101.705	105.222	100.446	106.073

☆U.S. GOVERNMENT PRINTING OFFICE: 1980-640-258-1872